

Adaptive Short-time Fourier Transform and Synchrosqueezing Transform for Non-stationary Signal Separation*

May 2, 2018

Lin Li¹, Haiyan Cai², Hongxia Han¹, Qingtang Jiang², and Hongbing Ji¹

1. School of Electronic Engineering, Xidian University, Xi'an 710071, P.R. China
2. Dept. of Math & CS, University of Missouri-St. Louis, St. Louis, MO 63121, USA

Abstract

The synchrosqueezing transform, a kind of reassignment method, aims to sharpen the time-frequency representation and to separate the components of a multicomponent non-stationary signal. In this paper, we consider the short-time Fourier transform (STFT) with a time-varying parameter. Based on the local approximation of linear frequency modulation mode, we analyze the well-separated condition of non-stationary multicomponent signals with this type STFT. In addition we propose the STFT-based synchrosqueezing transform (FSST) with a time-varying parameter, named the adaptive FSST, to enhance the time-frequency concentration and resolution of a multicomponent signal, and to separate its components more accurately. We also propose the 2nd-order adaptive FSST to further improve the adaptive FSST for the non-stationary signals with fast-varying frequencies. Furthermore, we present a localized optimization algorithm based on our well-separated condition to estimate the time-varying parameter adaptively and automatically. We also provide simulation results on synthetic signals and the bat echolocation signal to demonstrate the effectiveness and robustness of the proposed method.

1 Introduction

Recently the study of modeling a non-stationary signal as a superposition of locally band-limited, amplitude and frequency-modulated Fourier-like oscillatory modes has been a very active research area. Time-frequency analysis is widely used in engineering fields such as communication, radar and sonar as a powerful tool for analyzing time-varying non-stationary signals [1]. Time-frequency analysis is especially useful for signals containing many oscillatory components

*This work was supported in part by the National Natural Science Foundation of China (Grant No. 61201287) and Simons Foundation (Grant No. 353185)

with slowly time-varying amplitudes and instantaneous frequencies (IFs). The short-time Fourier transform (STFT), the continuous wavelet transform (CWT) and the Wigner-Ville distribution are the most typical time-frequency analysis, see details in [1]-[3]. The Wigner-Ville distribution is a type of bilinear time-frequency representation, and hence introduces cross-terms between multiple components, and cannot be used for the reconstruction of individual components. On the other hand, STFT and CWT are linear time-frequency representations, which can be applied to component reconstruction. Due to the uncertainty principle [2, 4], there is a trade-off between time resolution and frequency resolution for STFT and CWT. To overcome the limitation, a number of new time-frequency analysis methods have been proposed, such as the Hilbert spectrum analysis with empirical mode decomposition (EMD) [5], the reassignment method [6] and synchrosqueezed wavelet transform [7]. EMD is a data-driven decomposition algorithm which separates the time series signal into a set of monocomponents, called intrinsic mode functions (IMFs) [5]. EMD has studied by many researchers and has been used in many applications, see e.g. [8]-[16]. Because of the presence of widely disparate scales in a single IMF, or a similar scale residing in different IMF components, named as mode mixing [14], two close IMFs are hardly distinguished by EMD. The CWT-based synchrosqueezing transform (WSST), introduced in [7] and further studied in [17], is a special case of reassignment methods, which aims to sharpen the time-frequency representation by allocation the coefficient value to a different point in the time-frequency plane. A variant of WSST, STFT-based SST (FSST) is proposed in [18] and also studied in [19]. Similar to the CWT-based SST (WSST), FSST is a post processing technique to sharpen the STFT plane, which was proved to be robust to noise and small perturbations [20, 21]. But for frequency-varying signals, the squeezing effect of FSST is not well. In this regard, a 2nd-order FSST is introduced in [22, 23] to adapt to frequency modulated modes, and further theoretically analyzed in [24]. The 2nd-order FSST improves the concentration of the time-frequency representation well on perturbed linear chirps with Gaussian modulated amplitudes. The higher-order FSST is presented in [25], which aims to handle signals containing more general types. Other SST related methods include the generalized SST [26], a hybrid EMT-SST computational scheme [27], the synchrosqueezed wave packet transform [28], SST with vanishing moment wavelets [29], the multitapered SST [30] and the demodulation-transform based SST [31, 32]. The signal separation operator which is related to FSST was studied in [33] and an empirical signal separation algorithm was proposed in [34].

Most of the FSST algorithms available in the literature are based on STFT with a fixed window, which means high time resolution and frequency resolution cannot be obtained simultaneously. For broadband signals, a wide window is suitable for the low-frequency parts. On the contrary, a narrow window is suitable for the high-frequency parts. To enhance the time-frequency resolution and energy concentration, we propose the adaptive FSST and the 2nd-order adaptive FSST with a time-varying adaptive Gaussian window. The main innovations in this

paper are: (i) the well-separated condition for multicomponent signals are updated by using the linear frequency modulation to approximate a non-stationary signal during any local time, along with a new definition of bandwidth of Gaussian window, (ii) the adaptive window is defined for FSST and the corresponding signal recovery algorithm is proposed based on the adaptive FSST and 2nd-order adaptive FSST, and (iii) a localized optimization method based on the proposed well-separated condition is proposed to estimate the time-varying adaptive window width.

The idea of using an optimal time-varying window parameter (window width) has been studied or considered extensively in the literature, see e.g. [35]-[39]. In particular, the authors in [39] introduced a method to select the time-varying window width for sharp SST representation by minimizing the Rényi entropy. Furthermore, the window width of the signal separation operator algorithm in [33] is also time-varying. In addition, after we completed our work, we were aware of the very recent work [40] on the adaptive STFT-based SST with the window function containing time and frequency parameters. Our motivation is different from them in that we do not focus on the optimal parameter such that the corresponding STFT or IF has the sharpest representation in the time-frequency plane. Instead, we pursue the establishment of the well-separated condition for multicomponent signals based on the adaptive STFT and propose how to select window width $\sigma(t)$ such that STFTs of the components lie in non-overlapping regions of the time-frequency plane based on our established well-separated condition. The selected $\sigma(t)$ does not necessarily result in a sharp representation of the associated STFT. Instead, it is selected in such a way that the FSSTs of the components are well separated and hence the components can be recovered more accurately than those recovered by the conventional FSST.

The remainder of this paper is organized as follows. In Section 2 we provides a briefly review of FSST. We introduce the adaptive STFT and adaptive FSST with a time-varying parameter in Section 3, where we also introduce the 2nd-order adaptive FSST. We derive the optimal time-varying parameter for a monocomponent signal based on the linear-chirp model in Section 4. In Section 5, we establish the well-separated condition for multicomponent signals based on the adaptive STFT of linear chirps. In Section 6 we propose a localized optimization method on selection of window parameters based on the well-separated condition. Experiment results are provided in Section 7. Finally we give the conclusion in Section 8.

2 Short-time Fourier transform-based synchrosqueezed transform

In this section we briefly review the short-time Fourier transform-based synchrosqueezed transform (FSST). The (modified) short-time Fourier transform of $x(t) \in L_2(\mathbb{R})$ with a window function

$g(t) \in L_2(\mathbb{R})$ is defined by

$$V_x(t, \eta) = \int_{-\infty}^{\infty} x(\tau)g(\tau - t)e^{-i2\pi\eta(\tau - t)}d\tau \quad (1)$$

$$= \int_{-\infty}^{\infty} x(t + \tau)g(\tau)e^{-i2\pi\eta\tau}d\tau, \quad (2)$$

where t and η are the time variable and the frequency variable respectively. One can verify that STFT can be written as

$$V_x(t, \eta) = \int_{-\infty}^{\infty} \hat{x}(\xi)\hat{g}(\eta - \xi)e^{i2\pi t\xi}d\xi \quad (3)$$

where for a signal $x(t)$, its Fourier transform $\hat{x}(\xi)$ is defined by

$$\hat{x}(\xi) = \int_{-\infty}^{\infty} x(t)e^{-i2\pi\xi t}dt.$$

The original signal $x(t)$ can be recovered back from its STFT:

$$x(t) = \frac{1}{\|g\|_2^2} \int_{-\infty}^{\infty} \int_{-\infty}^{\infty} V_x(t, \eta)\overline{g(t - \tau)}e^{-i2\pi\eta(\tau - t)}d\tau d\eta.$$

If $g(0) \neq 0$, then one can show that $x(t)$ can also be recovered back from its STFT $V_x(t, \eta)$ with integrals involving only η :

$$x(t) = \frac{1}{g(0)} \int_{-\infty}^{\infty} V_x(t, \eta)d\eta. \quad (4)$$

In addition, if the window function $g(t) \in L_2(\mathbb{R})$ is real, then for a real-valued $x(t) \in L_2(\mathbb{R})$, we have

$$x(t) = \frac{2}{g(0)} \text{Re} \left(\int_0^{\infty} V_x(t, \eta)d\eta \right). \quad (5)$$

Here we remark that if the window function $g(t)$ is in the Schwarz class \mathcal{S} , then STFT $V_x(t, \eta)$ of a slowly growing $x(t)$ with $g(t)$ is well defined. Furthermore, the above formulas still hold.

STFT-based synchrosqueezing transform (FSST) The idea of FSST is to reassign the frequency variable. For a signal $x(t)$, at (t, η) for which $V_x(t, \eta) \neq 0$, denote

$$\omega_x(t, \eta) = \frac{\frac{\partial}{\partial t} V_x(t, \eta)}{2\pi i V_x(t, \eta)}. \quad (6)$$

The quantity $\omega_x(t, \eta)$ is called the “phase transformation” [17]. FSST is to reassign the frequency variable η by transforming STFT $V_x(t, \eta)$ of $x(t)$ to a quantity, denoted by $R_x(t, \eta)$, on the time-frequency plane:

$$R_x(t, \xi) = \int_{\{\zeta: V_x(t, \zeta) \neq 0\}} V_x(t, \zeta)\delta(\omega_x(t, \zeta) - \xi)d\zeta, \quad (7)$$

where ξ is the frequency variable.

From (4) and (5), we know the input signal $x(t)$ can be recovered from its FSST. More precisely, let $g(t) \in L_2(\mathbb{R})$ be a window function with $g(0) \neq 0$. Then for $x(t) \in L_2(\mathbb{R})$,

$$x(t) = \frac{1}{g(0)} \int_{-\infty}^{\infty} R_x(t, \xi) d\xi. \quad (8)$$

If in addition, $g(t)$ and $x(t)$ are real-valued, then

$$x(t) = \frac{2}{g(0)} \operatorname{Re} \left(\int_0^{\infty} R_x(t, \xi) d\xi \right). \quad (9)$$

For a multicomponent signal $x(t)$ given by

$$x(t) = \sum_{k=1}^K x_k(t) = \sum_{k=1}^K A_k(t) e^{i2\pi\phi_k(t)}, \quad (10)$$

when $A_k(t), \phi_k(t)$ satisfy certain conditions, each component $x_k(t)$ can be recovered from its FSST:

$$x_k(t) \approx \frac{1}{g(0)} \int_{|\xi - \phi'_k(t)| < \Gamma} R_x(t, \xi) d\xi, \quad (11)$$

for certain $\Gamma > 0$. For more mathematically precise definition of FSST and the conditions on $A_k(t), \phi_k(t)$ for (11), see [18, 19].

3 STFT and FSST with a time-varying parameter

3.1 Adaptive STFT and FSST with a time-varying parameter

We consider the window function given by

$$g_{\sigma}(t) = \frac{1}{\sigma} g\left(\frac{t}{\sigma}\right), \quad (12)$$

where $\sigma > 0$ is a parameter, $g(t)$ is a positive function in $L_2(\mathbb{R})$ with $g(0) \neq 0$ and having certain decaying order as $t \rightarrow \infty$. If

$$g(t) = \frac{1}{\sqrt{2\pi}} e^{-\frac{t^2}{2}}, \quad (13)$$

then $g_{\sigma}(t)$ is the Gaussian window function. The parameter σ is also called the window width in the time-domain of the window function $g_{\sigma}(t)$ since the time duration $\Delta_{g_{\sigma}}$ of g_{σ} is σ (up to a constant): $\Delta_{g_{\sigma}} = \sigma \Delta_g$. The parameter σ affects the shape of g_{σ} and hence, the representation of STFT of a signal with g_{σ} . On the other hand, [20] indicates that for a multicomponent signal as given in (10), if STFTs $V_{x_{k-1}}(t, \eta)$ and $V_{x_k}(t, \eta)$ of two components x_{k-1} and x_k are mixed, then FSST cannot separate these two components $x_{k-1}(t)$ and $x_k(t)$ either. Thus it is desirable that appropriate σ can be chosen so that STFTs of different components do not overlap. In this paper we introduce STFT with a time-varying parameter and then establish the separability condition of a multicomponent signal based on this new type of STFT.

For a signal $x(t)$, we define STFT of $x(t)$ with a time-varying parameter as

$$\tilde{V}_x(t, \eta) = V_s(t, \eta, \sigma(t)) := \int_{-\infty}^{\infty} x(\tau) g_{\sigma(t)}(\tau - t) e^{-i2\pi\eta(\tau - t)} d\tau \quad (14)$$

$$= \int_{-\infty}^{\infty} x(t + \tau) \frac{1}{\sigma(t)} g\left(\frac{\tau}{\sigma(t)}\right) e^{-i2\pi\eta\tau} d\tau. \quad (15)$$

where σ is a positive function of t . Sometimes we also use $V_s(t, \eta, \sigma(t))$ to denote the STFT of $x(t)$ with a time-varying parameter. We call $\tilde{V}_x(t, \eta)$ the adaptive STFT of $x(t)$ with g_σ . It is easy to obtain

$$\tilde{V}_x(t, \eta) = \int_{-\infty}^{\infty} \hat{x}(\xi) \hat{g}_{\sigma(t)}(\eta - \xi) e^{i2\pi t\xi} d\xi = \int_{-\infty}^{\infty} \hat{x}(\xi) \hat{g}(\sigma(t)(\eta - \xi)) e^{i2\pi t\xi} d\xi$$

We can obtain that $x(t)$ can be recovered from $\tilde{V}_x(t, \eta)$ by formulas similar to (4) and (5).

Theorem 1. *Let $\tilde{V}_x(t, \eta)$ be the time-varying STFT of $x(t) \in L_2(\mathbb{R})$ defined by (14). Then*

$$x(t) = \frac{\sigma(t)}{g(0)} \int_{-\infty}^{\infty} \tilde{V}_x(t, \eta) d\eta. \quad (16)$$

If in addition $g(t)$ is real-valued, then for a real-valued $x(t)$, we have

$$x(t) = \frac{2\sigma(t)}{g(0)} \operatorname{Re} \left(\int_0^{\infty} \tilde{V}_x(t, \eta) d\eta \right). \quad (17)$$

The proof of Theorem 1 is presented in Appendix.

Next we consider the synchrosqueezing transform (SST) associated with the adaptive STFT. First we need to define the phase transformation ω_x^{adp} associated with the adaptive STFT. Let $g_\sigma(t)$ be the window function defined by (12). Let $g_\sigma^2(t) = \frac{t}{\sigma^2} g'(\frac{t}{\sigma})$. In the following we use $\tilde{V}_x^{g^2}(t, \eta)$ to denote STFT defined by (14) with $g_{\sigma(t)}$ replaced by $g_{\sigma(t)}^2$, namely,

$$\tilde{V}_x^{g^2}(t, \eta) := \int_{-\infty}^{\infty} x(t + \tau) \frac{\tau}{\sigma^2(t)} g'\left(\frac{\tau}{\sigma(t)}\right) e^{-i2\pi\eta\tau} d\tau. \quad (18)$$

To define the phase transformation ω_x^{adp} , we first consider $s(t) = Ae^{i2\pi ct}$. From

$$\tilde{V}_s(t, \eta) = \int_{-\infty}^{\infty} s(t + \tau) g_{\sigma(t)}(t) e^{-i2\pi\eta\tau} d\tau = A \int_{-\infty}^{\infty} e^{i2\pi c(t+\tau)} \frac{1}{\sigma(t)} g\left(\frac{\tau}{\sigma(t)}\right) e^{-i2\pi\eta\tau} d\tau,$$

we have

$$\begin{aligned} \frac{\partial}{\partial t} \tilde{V}_s(t, \eta) &= A \int_{-\infty}^{\infty} (i2\pi c) e^{i2\pi c(t+\tau)} \frac{1}{\sigma(t)} g\left(\frac{\tau}{\sigma(t)}\right) e^{-i2\pi\eta\tau} d\tau \\ &\quad + A \int_{-\infty}^{\infty} e^{i2\pi c(t+\tau)} \left(-\frac{\sigma'(t)}{\sigma(t)^2}\right) g\left(\frac{\tau}{\sigma(t)}\right) e^{-i2\pi\eta\tau} d\tau + A \int_{-\infty}^{\infty} e^{i2\pi c(t+\tau)} \left(-\frac{\sigma'(t)\tau}{\sigma(t)^3}\right) g'\left(\frac{\tau}{\sigma(t)}\right) e^{-i2\pi\eta\tau} d\tau \\ &= i2\pi c \tilde{V}_s(t, \eta) - \frac{\sigma'(t)}{\sigma(t)} \tilde{V}_s(t, \eta) - \frac{\sigma'(t)}{\sigma(t)} \tilde{V}_s^{g^2}(t, \eta). \end{aligned}$$

Thus, if $\tilde{V}_s(t, \eta) \neq 0$, we have

$$\frac{\frac{\partial}{\partial t} \tilde{V}_s(t, \eta)}{i2\pi \tilde{V}_s(t, \eta)} = c - \frac{\sigma'(t)}{i2\pi \sigma(t)} - \frac{\sigma'(t)}{\sigma(t)} \frac{\tilde{V}_s^{g^2}(t, \eta)}{i2\pi \tilde{V}_s(t, \eta)}.$$

Therefore, the IF of $s(t)$, which is c , can be obtained by

$$c = \operatorname{Re} \left\{ \frac{\frac{\partial}{\partial t} \tilde{V}_s(t, \eta)}{i2\pi \tilde{V}_s(t, \eta)} \right\} + \frac{\sigma'(t)}{\sigma(t)} \operatorname{Re} \left\{ \frac{\tilde{V}_s^{g^2}(t, \eta)}{i2\pi \tilde{V}_s(t, \eta)} \right\}. \quad (19)$$

Hence, for a general $x(t)$, at (t, η) for which $\tilde{V}_x(t, \eta) \neq 0$, the quantity in the right-hand side of the above equation is a good candidate for the IF of x . This quantity is also called the phase transformation, and we denote it by $\omega_x^{adp}(t, \eta)$:

$$\omega_x^{adp}(t, \eta) = \operatorname{Re} \left\{ \frac{\partial_t(\tilde{V}_x(t, \eta))}{i2\pi \tilde{V}_x(t, \eta)} \right\} + \frac{\sigma'(t)}{\sigma(t)} \operatorname{Re} \left\{ \frac{\tilde{V}_x^{g^2}(t, \eta)}{i2\pi \tilde{V}_x(t, \eta)} \right\}, \quad \text{for } \tilde{V}_x(t, \eta) \neq 0. \quad (20)$$

The FSST with a time-varying parameter (called the adaptive FSST of $x(t)$) is defined by

$$R_x^{adp}(t, \xi) := \int_{\{\eta \in \mathbb{R}: \tilde{V}_x(t, \eta) \neq 0\}} \tilde{V}_x(t, \eta) \delta(\omega_x^{adp}(t, \eta) - \xi) d\eta, \quad (21)$$

where ξ is the frequency variable. The reconstruction formulas in (16) and (17) lead to that $x(t)$ can be reconstructed from its adaptive FSST as presented in the following theorem.

Theorem 2. *Let $R_x^{adp}(t, \xi)$ be the adaptive FSST of $x(t)$ defined by (21). Then*

$$x(t) = \frac{\sigma(t)}{g(0)} \int_{-\infty}^{\infty} R_x^{adp}(t, \xi) d\xi. \quad (22)$$

If in addition $g(t)$ is real-valued, then for real-valued $x(t)$, we have

$$x(t) = \frac{2\sigma(t)}{g(0)} \operatorname{Re} \left(\int_0^{\infty} R_x^{adp}(t, \xi) d\xi \right). \quad (23)$$

One can use the following formula to recover the k th component $x_k(t)$ of a multicomponent signal from the adaptive FSST:

$$x_k(t) = \frac{2\sigma(t)}{g(0)} \operatorname{Re} \left(\int_{|\xi - \phi'_k(t)| < \Gamma} R_x^{adp}(t, \xi) d\eta \right). \quad (24)$$

for some $\Gamma > 0$.

Here we remark that if g is the Gaussian function, then the second term on the right side of (19) disappears. Indeed, in this case, for $s(t) = Ae^{i2\pi ct}$, we have

$$\begin{aligned} \tilde{V}_s(t, \eta) &= \int_{-\infty}^{\infty} Ae^{i2\pi c(t+\tau)} g_{\sigma(t)}(\tau) e^{-i2\pi \eta \tau} d\tau \\ &= Ae^{i2\pi tc} \hat{g}_{\sigma(t)}(\eta - c) \\ &= Ae^{i2\pi tc} e^{-2\pi^2 \sigma(t)^2 (\eta - c)^2}. \end{aligned}$$

Observe that

$$\begin{aligned}\frac{\partial}{\partial t} \tilde{V}_s(t, \eta) &= i2\pi c A e^{i2\pi t c} e^{-2\pi^2 \sigma(t)^2 (\eta - c)^2} + A e^{i2\pi t c} e^{-2\pi^2 \sigma(t)^2 (\eta - c)^2} (-4\pi^2) (\eta - c)^2 \sigma(t) \sigma(t)' \\ &= i2\pi c \tilde{V}_s(t, \eta) + \tilde{V}_s(t, \eta) (-4\pi^2) (\eta - c)^2 \sigma(t) \sigma(t)'.\end{aligned}$$

Thus, we have

$$\frac{\frac{\partial}{\partial t} \tilde{V}_s(t, \eta)}{i2\pi \tilde{V}_s(t, \eta)} = c + i 2\pi (\eta - c)^2 \sigma(t) \sigma(t)'.$$

Since both c and $2\pi(\eta - c)^2 \sigma(t) \sigma(t)'$ are real, the IF c of $s(t)$ can be obtained by

$$c = \text{Re} \left\{ \frac{\partial_t (\tilde{V}_s(t, \eta))}{i2\pi \tilde{V}_s(t, \eta)} \right\}.$$

Hence if g is the Gaussian function, for a general signal $x(t)$, we may define the phase transformation by

$$\tilde{\omega}_x(t, \eta) = \text{Re} \left\{ \frac{\partial_t (\tilde{V}_x(t, \eta))}{i2\pi \tilde{V}_x(t, \eta)} \right\}, \quad \text{for } \tilde{V}_x(t, \eta) \neq 0.$$

3.2 Second-order adaptive FSST

The 2nd-order SST was introduced in [22]. The main idea is to define a new phase transformation ω_x^{2nd} such that when $x(t)$ is a linear frequency modulation (LFM) signal, then ω_x^{2nd} is exactly the IF of $x(t)$. We say $s(t)$ is an LFM signal or a linear chirp if

$$s(t) = A(t) e^{i2\pi \phi(t)} = A e^{pt + \frac{q}{2} t^2} e^{i2\pi (ct + \frac{1}{2} rt^2)} \quad (25)$$

with phase function $\phi(t) = ct + \frac{1}{2} rt^2$, IF $\phi'(t) = c + rt$ and chirp rate $\phi''(t) = r$, IA $A(t) = A e^{pt + \frac{q}{2} t^2}$, where p, q are real numbers and $|p|$ and $|q|$ are much smaller than c . In [22], the reassignment operators are used to derive ω_s^{2nd} . Here our phase transform ω_s^{2nd} is derived without using the reassignment operators and it is also slightly different from that in [22]. Our derivation can easily be generalized to the case of adaptive STFT and FSST. In the following we show how to derive ω_s^{2nd} .

For a given window function g , let $V_s(t, \eta)$ be STFT of $s(t)$ with g defined by (1). For $u_1(t) = tg(t)$, let $V_s^{u_1}(t, \eta)$ denote STFT of $s(t)$ with $u_1(t)$, namely, the integral on the right-hand side of (1) with $x(t)$ and $g(t)$ replaced by $s(t)$ and $u_1(t)$ respectively.

Observe that for $s(t)$ given by (25)

$$s'(t) = (p + qt + i2\pi(c + rt))s(t).$$

Thus from

$$V_s(t, \eta) = \int_{-\infty}^{\infty} s(t + \tau) g(\tau) e^{-i2\pi \eta \tau} d\tau,$$

we have

$$\begin{aligned}
\frac{\partial}{\partial t} V_s(t, \eta) &= \int_{-\infty}^{\infty} s'(t + \tau) g(\tau) e^{-i2\pi\eta\tau} d\tau \\
&= \int_{-\infty}^{\infty} (p + q(t + \tau) + i2\pi(c + rt + r\tau)) s(t + \tau) g(\tau) e^{-i2\pi\eta\tau} d\tau \\
&= (p + qt + i2\pi(c + rt)) V_s(t, \eta) + (q + i2\pi r) V_s^{u1}(t, \eta).
\end{aligned}$$

Thus at (t, η) on which $V_s(t, \eta) \neq 0$, we have

$$\frac{\frac{\partial}{\partial t} V_s(t, \eta)}{V_s(t, \eta)} = p + qt + i2\pi(c + rt) + (q + i2\pi r) \frac{V_s^{u1}(t, \eta)}{V_s(t, \eta)}. \quad (26)$$

Taking partial derivative $\frac{\partial}{\partial \eta}$ to both sides of (26), we have

$$\frac{\partial}{\partial \eta} \left(\frac{\frac{\partial}{\partial t} V_s(t, \eta)}{V_s(t, \eta)} \right) = (q + i2\pi r) \frac{\partial}{\partial \eta} \left(\frac{V_s^{u1}(t, \eta)}{V_s(t, \eta)} \right).$$

Thus if $\frac{\partial}{\partial \eta} \left(\frac{V_s^{u1}(t, \eta)}{V_s(t, \eta)} \right) \neq 0$, then $q + i2\pi r = p_0(t, \eta)$, where

$$p_0(t, \eta) = \frac{1}{\frac{\partial}{\partial \eta} \left(\frac{V_s^{u1}(t, \eta)}{V_s(t, \eta)} \right)} \frac{\partial}{\partial \eta} \left(\frac{\frac{\partial}{\partial t} V_s(t, \eta)}{V_s(t, \eta)} \right).$$

Back to (26), we have

$$\frac{\frac{\partial}{\partial t} V_s(t, \eta)}{V_s(t, \eta)} = p + qt + i2\pi(c + rt) + \frac{V_s^{u1}(t, \eta)}{V_s(t, \eta)} p_0(t, \eta).$$

Thus,

$$\phi'(t) = c + rt = \frac{\frac{\partial}{\partial t} V_s(t, \eta)}{i2\pi V_s(t, \eta)} - \frac{p + qt}{i2\pi} - \frac{V_s^{u1}(t, \eta)}{i2\pi V_s(t, \eta)} p_0(t, \eta).$$

Since $\phi'(t)$ is real, taking the real parts of the quantities in the above equation, we have

$$\phi'(t) = c + rt = \operatorname{Re} \left\{ \frac{\frac{\partial}{\partial t} V_s(t, \eta)}{i2\pi V_s(t, \eta)} \right\} - \operatorname{Re} \left\{ \frac{V_s^{u1}(t, \eta)}{i2\pi V_s(t, \eta)} p_0(t, \eta) \right\}.$$

Hence, for a signal $x(t)$, one may define the phase transformation as

$$\omega_x^{2nd}(t, \eta) = \begin{cases} \operatorname{Re} \left\{ \frac{\frac{\partial}{\partial t} V_x(t, \eta)}{i2\pi V_x(t, \eta)} \right\} - \operatorname{Re} \left\{ \frac{V_x^{u1}(t, \eta)}{i2\pi V_x(t, \eta)} p_0(t, \eta) \right\}, & \text{if } \frac{\partial}{\partial \eta} \left(\frac{V_x^{u1}(t, \eta)}{V_x(t, \eta)} \right) \neq 0, V_x(t, \eta) \neq 0, \\ \operatorname{Re} \left\{ \frac{\frac{\partial}{\partial t} V_x(t, \eta)}{i2\pi V_x(t, \eta)} \right\}, & \text{if } \frac{\partial}{\partial \eta} \left(\frac{V_x^{u1}(t, \eta)}{V_x(t, \eta)} \right) = 0, V_x(t, \eta) \neq 0. \end{cases} \quad (27)$$

From the above derivation, we know $\omega_x^{2nd}(t, \eta)$ is exactly the IF $\phi'(t)$ of $x(t)$ if $x(t)$ is an LFM signal given by (25).

Next we consider the STFT with a time-varying parameter. Let $g_\sigma(t)$ be the window function defined by (12). As in Section 3.1, denote $g_\sigma^2(t) = \frac{t}{\sigma^2} g'(\frac{t}{\sigma})$, and let $\tilde{V}_x^{g^2}(t, \eta)$ denote the adaptive STFT defined by (18). In addition, we define

$$g_\sigma^1(t) = \frac{t}{\sigma} g_\sigma(t) = \frac{t}{\sigma^2} g\left(\frac{t}{\sigma}\right)$$

and we use $\tilde{V}_x^{g^1}(t, \eta)$ to denote the STFT defined by (14) with $g_{\sigma(t)}$ replaced by $g_{\sigma(t)}^1$, namely,

$$\tilde{V}_x^{g^1}(t, \eta) := \int_{-\infty}^{\infty} x(t) g_{\sigma(t)}^1(\tau - t) e^{-i2\pi\eta(\tau - t)} d\tau = \int_{-\infty}^{\infty} x(t + \tau) \frac{\tau}{\sigma^2(t)} g\left(\frac{\tau}{\sigma(t)}\right) e^{-i2\pi\eta\tau} d\tau. \quad (28)$$

One can obtain that

$$\hat{g}_\sigma^1(\xi) = \frac{i}{2\pi} (\hat{g})'(\sigma(\xi - \mu)).$$

For a signal $x(t)$, we define the phase transformation for the 2nd-order adaptive FSST as

$$\omega_x^{adp, 2nd}(t, \eta) = \begin{cases} \operatorname{Re}\left\{\frac{\partial}{\partial t} \tilde{V}_x(t, \eta)\right\} + \frac{\sigma'(t)}{\sigma(t)} \operatorname{Re}\left\{\frac{\tilde{V}_x^{g^2}(t, \eta)}{i2\pi \tilde{V}_x(t, \eta)}\right\} - \operatorname{Re}\left\{\frac{\tilde{V}_x^{g^1}(t, \eta)}{i2\pi \tilde{V}_x(t, \eta)} P_0(t, \eta)\right\}, \\ \quad \text{if } \frac{\partial}{\partial \eta} \left(\frac{\tilde{V}_x^{g^1}(t, \eta)}{\tilde{V}_x(t, \eta)}\right) \neq 0 \text{ and } \tilde{V}_x(t, \eta) \neq 0; \\ \operatorname{Re}\left\{\frac{\partial}{\partial t} \tilde{V}_x(t, \eta)\right\} + \frac{\sigma'(t)}{\sigma(t)} \operatorname{Re}\left\{\frac{\tilde{V}_x^{g^2}(t, \eta)}{i2\pi \tilde{V}_x(t, \eta)}\right\}, \text{ if } \frac{\partial}{\partial \eta} \left(\frac{\tilde{V}_x^{g^1}(t, \eta)}{\tilde{V}_x(t, \eta)}\right) = 0, \tilde{V}_x(t, \eta) \neq 0, \end{cases} \quad (29)$$

where

$$P_0(t, \eta) = \frac{1}{\frac{\partial}{\partial \eta} \left(\frac{\tilde{V}_x^{g^1}(t, \eta)}{\tilde{V}_x(t, \eta)}\right)} \left\{ \frac{\partial}{\partial \eta} \left(\frac{\partial}{\partial t} \tilde{V}_x(t, \eta)\right) + \frac{\sigma'(t)}{\sigma(t)} \frac{\partial}{\partial \eta} \left(\frac{\tilde{V}_x^{g^2}(t, \eta)}{\tilde{V}_x(t, \eta)}\right) \right\}. \quad (30)$$

Then we have the following theorem with its proof given in Appendix.

Theorem 3. *If $x(t)$ is an LFM signal given by (25), then at (t, η) where $\frac{\partial}{\partial \eta} \left(\frac{\tilde{V}_x^{g^1}(t, \eta)}{\tilde{V}_x(t, \eta)}\right) \neq 0$ and $\tilde{V}_x(t, \eta) \neq 0$, $\omega_x^{adp, 2nd}(t, \eta)$ defined by (29) is the IF of $x(t)$, namely $\omega_x^{adp, 2nd}(t, \eta) = c + rt$.*

Observe that when $\sigma = \sigma(t)$ is a constant function, $\omega_x^{adp, 2nd}(t, \eta)$ is reduced to $\omega_x^{2nd}(t, \eta)$ in (27).

With the phase transformation $\omega_x^{adp, 2nd}(t, \eta)$ in (29), we define the 2nd-order FSST with a time-varying parameter, called the 2nd-order adaptive FSST, of a signal $x(t)$ as in (21):

$$R_x^{adp, 2nd}(\xi, t) := \int_{\{\eta \in \mathbb{R}: \tilde{V}_x(t, \eta) \neq 0\}} \tilde{V}_x(t, \eta) \delta(\omega_x^{adp, 2nd}(t, \eta) - \xi) d\eta, \quad (31)$$

where ξ is the frequency variable. We also have the reconstruction formulas for $x(t)$ and $x_k(t)$ similar to (22), (23) and (24) with $R_x^{adp}(\xi, t)$ replaced by $R_x^{adp, 2nd}(\xi, t)$.

4 Support zones of STFTs of LFM signals

The article [20] studies the relation between CWT and WSST, and that between STFT and FSST as well. For a multicomponent signal as given in (10), [20] notes that if CWTs $W_{x_{k-1}}(t, \eta)$ and $W_{x_k}(t, \eta)$ of two components are mixed, then WSST is unable to separate these two components $x_{k-1}(t)$ and $x_k(t)$ either. This also happens for STFT and FSST. The parameter σ for the window function g_σ affects the sharpness of STFT of a signal. In this section, we study how the time-varying parameter $\sigma(t)$ controls the representation of STFT $\tilde{V}_x(t, \eta)$ and provide the parameter

$\sigma(t)$ with which STFT has the sharpest representation in the time-frequency plane. In the next section, we will consider the problem that under which condition, if any, for a multicomponent signal as given in (10), with a suitable choice of $\sigma(t)$, the STFTs of $\tilde{V}_{x_k}(t, \eta)$, $1 \leq k \leq K$ are well separated, and hence, the associated FSST has a sharper representation than the conventional FSST and the components x_k can be recovered more accurately.

To study the sharpness of STFT of a monocomponent signal or the separability of STFTs (including STFTs with a time-varying parameter) of different components x_k of $x(t)$, we need to consider the support zone of STFTs in the time-frequency plane, the region outside which STFT ≈ 0 . For $s(t) = Ae^{i2\pi ct}$, its STFT $V_s(t, \eta)$ is $Ae^{i2\pi tc}\hat{g}(\eta - c)$. Thus the support zone of $V_s(t, \eta)$ in the time-frequency plane is determined by the support of \hat{g} outside which $\hat{g}(\xi) \approx 0$. Therefore, first of all, we need to define the “support” of \hat{g} . More precise, for a given threshold $0 < \epsilon < 1$, if $|\hat{g}(\xi)|/\max_{\xi} |\hat{g}(\xi)| < \epsilon$ for $|\xi| \geq \xi_0$, then we say $\hat{g}(\xi)$ is “supported” in $[-\xi_0, \xi_0]$. We use $L_{\hat{g}} = 2\xi_0$ to denote the length of the “support” interval of \hat{g} and we call it the duration of \hat{g} .

In the rest of this paper, we consider g given by (13) and thus $g_{\sigma}(t)$ is the Gaussian window function defined by

$$g_{\sigma}(t) = \frac{1}{\sigma\sqrt{2\pi}}e^{-\frac{t^2}{2\sigma^2}}, \quad (32)$$

with its Fourier transform given by

$$\hat{g}_{\sigma}(\xi) = e^{-2\pi^2\sigma^2\xi^2}. \quad (33)$$

For g given by (13), $|\hat{g}(\xi)| = e^{-2\pi^2\xi^2} < \epsilon$ if and only if $|\xi| > \alpha$, where

$$\alpha = \frac{1}{2\pi}\sqrt{2\ln(1/\epsilon)}. \quad (34)$$

Thus we regard that \hat{g} is “supported” in $[-\alpha, \alpha]$. Hence, \hat{g}_{σ} , defined by (33), is “supported” in $[-\frac{\alpha}{\sigma}, \frac{\alpha}{\sigma}]$, and $L_{\hat{g}_{\sigma}} = \frac{2\alpha}{\sigma}$.

For $s(t) = Ae^{i2\pi ct}$, since its STFT with g_{σ} is

$$V_s(t, \eta) = Ae^{i2\pi tc}\hat{g}_{\sigma}(\eta - c),$$

and $\hat{g}_{\sigma}(\eta - c)$ is “supported” in $c - \frac{\alpha}{\sigma} \leq \eta \leq c + \frac{\alpha}{\sigma}$, $V_s(t, \eta)$ concentrates around $\eta = c$ and lies within the zone (a strip) of the time-frequency plane (t, η) :

$$\{(t, \eta) : c - \frac{\alpha}{\sigma} \leq \eta \leq c + \frac{\alpha}{\sigma}, t \in \mathbb{R}\}. \quad (35)$$

Next we consider the LFM signal. We start with a simple version of (25):

$$s_1(t) = Ae^{i2\pi(ct + \frac{1}{2}rt^2)}. \quad (36)$$

Here we assume $\phi'(t) = c + rt > 0$. First we find STFT of the LFM signals.

Proposition 1. Let $s_1(t)$ be the linear chirp signal given by (36). The STFT of $s_1(t)$ with the Gaussian window function $g_\sigma(t)$ is given by

$$V_{s_1}(t, \eta) = \frac{A}{\sqrt{1 - i2\pi\sigma^2 r}} e^{i2\pi(ct+rt^2/2)} h_1(\eta - (c + rt)), \quad (37)$$

where

$$h_1(\xi) = e^{-\frac{2\pi^2\sigma^2}{1+(2\pi r\sigma^2)^2}(1+i2\pi\sigma^2 r)\xi^2}.$$

The proof of Proposition 1 will be provided in Appendix. Observe that $|h_1(\xi)|$ is a Gaussian function with duration

$$L_{|h_1|} = 2\alpha\sqrt{\frac{1 + (2\pi r\sigma^2)^2}{\sigma^2}} = 2\alpha\sqrt{\frac{1}{\sigma^2} + (2\pi r\sigma)^2}.$$

Thus the ridge of $V_{s_1}(t, \eta)$ concentrates around $\eta = c + rt$ in the time-frequency plane, and $V_{s_1}(t, \eta)$ lies within the zone of time-frequency plane of (t, η) :

$$-\frac{1}{2}L_{|h_1|} \leq c + rt - \eta \leq \frac{1}{2}L_{|h_1|},$$

or equivalently

$$c + rt - \alpha\sqrt{\frac{1}{\sigma^2} + (2\pi r\sigma)^2} \leq \eta \leq c + rt + \alpha\sqrt{\frac{1}{\sigma^2} + (2\pi r\sigma)^2}. \quad (38)$$

$L_{|h_1|}$ gains its minimum when $\frac{1}{\sigma^2} = (2\pi r\sigma)^2$, namely,

$$\sigma = \frac{1}{\sqrt{2\pi|r|}} = \frac{1}{\sqrt{2\pi|\phi''(t)|}}. \quad (39)$$

The choice of σ given in (39) results in the sharpest representation of $V_{s_1}(t, \eta)$.

Next we consider the LFM signal $s(t)$ given by (25). We obtain (see Appendix) that its STFT with the Gaussian window function $g_\sigma(t)$ is

$$V_s(t, \eta) = \frac{A}{\sqrt{1 - q\sigma^2 - i2\pi\sigma^2 r}} e^{p+\frac{q}{2}t^2+i2\pi(ct+rt^2/2)} h(\eta - (c + rt)), \quad (40)$$

where

$$h(\xi) = e^{-2\pi^2(\xi - \frac{p+qt}{i2\pi})^2 \frac{\sigma^2}{1-q\sigma^2-i2\pi\sigma^2 r}}.$$

By direct calculations, we have

$$|h(\xi)| = e^{\frac{\sigma^2(p+qt)^2}{2(1-q\sigma^2)^2}} e^{-\frac{2\pi^2\sigma^2(1-q\sigma^2)}{(1-q\sigma^2)^2+(2\pi r\sigma^2)^2} \left(\xi - \frac{p+qt}{1-q\sigma^2} r\sigma^2\right)^2}.$$

Thus $|h(\xi)|$ is a Gaussian function with duration

$$L_{|h|} = 2\alpha\sqrt{\frac{(1-q\sigma^2)^2 + (2\pi r\sigma^2)^2}{\sigma^2(1-q\sigma^2)}} = 2\alpha\sqrt{\frac{1-q\sigma^2}{\sigma^2} + \frac{(2\pi r\sigma)^2}{1-q\sigma^2}}.$$

Therefore the ridge of $V_s(t, \eta)$ concentrates around $\eta = c + rt + \frac{p+qt}{1-q\sigma^2}r\sigma^2$ in the time-frequency plane, and $V_s(t, \eta)$ lies within the zone of time-frequency plane of (t, η) :

$$-\alpha\sqrt{\frac{1-q\sigma^2}{\sigma^2} + \frac{(2\pi r\sigma)^2}{1-q\sigma^2}} \leq c + rt + \frac{p+qt}{1-q\sigma^2}r\sigma^2 - \eta \leq \alpha\sqrt{\frac{1-q\sigma^2}{\sigma^2} + \frac{(2\pi r\sigma)^2}{1-q\sigma^2}}.$$

Since we assume p, q are very small, we may drop the terms with p, q , and hence, the time-frequency zone of $V_s(t, \eta)$ is reduced to that given by (38). In the following, for simplicity of presentation, we focus on the LFM signals given by (36) though our method/model can be applied to the LFM signals given by (25).

For a monocomponent signal $x(t) = A(t)e^{i2\pi\phi(t)}$, if its STFT with g_σ , which is also given by (refer to (2)),

$$V_x(t, \eta) = \int_{-\infty}^{\infty} A(t+\tau)e^{i2\pi\phi(t+\tau)}g_\sigma(\tau)e^{-i2\pi\eta\tau}d\tau$$

can be well approximated by

$$V_x(t, \eta) \approx \int_{-\infty}^{\infty} A(t)e^{i2\pi(\phi(t)+\phi'(t)\tau+\frac{1}{2}\phi''(t)\tau^2)}g_\sigma(\tau)e^{-i2\pi\eta\tau}d\tau,$$

then the choice of σ given

$$\sigma = \frac{1}{\sqrt{2\pi|\phi''(t)|}} \quad (41)$$

results in the sharpest representation of $V_x(t, \eta)$. The choice of $\sigma = \sigma(t)$ in (41) coincides the result derived in [1].

Observe that σ in (41) is the optimal parameter for the representation of a monocomponent signal. In the next section, we will use the obtained time-frequency zone in (38) for STFT of a linear chirp to study the well-separated condition for a multicomponent signal.

5 Separability of multicomponent signals and selection of time-varying parameter

In this section, we will consider the problem that under which condition, if any, for a multicomponent signal as given in (10), with a suitable choice of $\sigma(t)$, STFTs $\tilde{V}_{x_k}(t, \eta)$, $1 \leq k \leq K$ of different components x_k defined in (14) are well separated, and hence, the associated FSST has a sharper representation than the conventional FSST and the components x_k can be recovered more accurately.

First we consider the choice for $\sigma(t)$ based on the sinusoidal signal model. Recall that STFT of $s(t) = Ae^{i2\pi ct}$ with $g_\sigma(t)$ is supported in the zone of the time-frequency plane given by (35).

Suppose $x(t)$ is a finite summation of sinusoidal signals:

$$x(t) = \sum_{k=1}^K A_k e^{i2\pi c_k t}, \quad (42)$$

where A_k, c_k are positive constants with $0 < c_k < c_{k+1}$. Since the STFT of the k -component of $x(t)$ lies within the zone of the time-frequency plane (t, η) : $c_k - \alpha/\sigma \leq \eta \leq c_k + \alpha/\sigma$ for any t , the components of $x(t)$ will be well-separated in the time-frequency plane if

$$c_{k-1} + \frac{\alpha}{\sigma} \leq c_k - \frac{\alpha}{\sigma},$$

or equivalently

$$\sigma \geq \frac{2\alpha}{c_k - c_{k-1}}, \quad \text{for } k = 2, 3, \dots, K.$$

More general, for $x(t)$ given by (10), if for each k , the time-varying STFT of $x_k(t) = A_k(t)e^{i2\pi\phi_k(t)}$ with $g_{\sigma(t)}$, which is (refer to (15))

$$\int_{-\infty}^{\infty} A_k(t+\tau) e^{i2\pi\phi_k(t+\tau)} g_{\sigma(t)}(\tau) e^{-i2\pi\eta\tau} d\tau \quad (43)$$

can be well-approximated by

$$\int_{-\infty}^{\infty} A_k(t) e^{i2\pi(\phi_k(t) + \phi'_k(t)\tau)} g_{\sigma(t)}(\tau) e^{-i2\pi\eta\tau} d\tau,$$

then the well-separable condition for this $x(t)$ is

$$\sigma(t) \geq \frac{2\alpha}{\phi'_k(t) - \phi'_{k-1}(t)}, \quad \text{for } k = 2, 3, \dots, K$$

for each t .

We observe in our experiments that in general a big σ will result in low time-resolution and unreliable representation of the FSST of a signal $x(t)$. Actually, the error bounds derived in [17] imply that for a signal, its synchrosqueezed representation is sharper when the window width in the time domain of the window function g_{σ} , which is σ (up to a constant), is smaller. Thus we should choose $\sigma(t)$ as small as possible. Hence, we propose the sinusoidal signal-based choice for σ , denoted by $\sigma_1(t)$, to be

$$\sigma_1(t) = \max_{2 \leq k \leq K} \left\{ \frac{2\alpha}{\phi'_k(t) - \phi'_{k-1}(t)} \right\}. \quad (44)$$

In this paper we focus on the LFM model, namely, we will derive the well-separated condition based on the linear chirp model. More precisely, we consider $x(t) = \sum_{k=1}^K x_k(t)$, where each $x_k(t)$ is a linear chirp, namely,

$$x_k(t) = A_k e^{i2\pi(c_k t + \frac{1}{2} r_k t^2)}$$

with the phase $\phi_k(t) = c_k t + \frac{1}{2} r_k t^2$ and $\phi'_{k-1}(t) < \phi'_k(t)$.

From (38), STFT $V_{x_k}(t, \eta)$ of x_k with g_σ lies within the zone of time-frequency plane (t, η) :

$$c_k + r_k t - \alpha \sqrt{\frac{1}{\sigma^2} + (2\pi r_k \sigma)^2} \leq \eta \leq c_k + r_k t + \alpha \sqrt{\frac{1}{\sigma^2} + (2\pi r_k \sigma)^2}, \quad (45)$$

for all t . Since

$$\frac{\sqrt{2}}{2} \left(\frac{1}{\sigma} + 2\pi |r_k| \sigma \right) \leq \sqrt{\frac{1}{\sigma^2} + (2\pi |r_k| \sigma)^2} \leq \frac{1}{\sigma} + 2\pi |r_k| \sigma,$$

we replace the time-frequency zone of $V_{x_k}(t, \eta)$ in (45) by a larger zone for $V_{x_k}(t, \eta)$ by using $\frac{1}{\sigma} + 2\pi |r_k| \sigma$ to replace $\sqrt{\frac{1}{\sigma^2} + (2\pi |r_k| \sigma)^2}$:

$$c_k + r_k t - \alpha \left(\frac{1}{\sigma} + 2\pi |r_k| \sigma \right) \leq \eta \leq c_k + r_k t + \alpha \left(\frac{1}{\sigma} + 2\pi |r_k| \sigma \right). \quad (46)$$

Therefore, in this case, $x_{k-1}(t)$ and $x_k(t)$ are separable in the time-frequency plane if

$$c_{k-1} + r_{k-1} t + \alpha \left(\frac{1}{\sigma} + 2\pi |r_{k-1}| \sigma \right) \leq c_k + r_k t - \alpha \left(\frac{1}{\sigma} + 2\pi |r_k| \sigma \right).$$

More general, for $x(t)$ given by (10), if for each k , the time-varying STFT $\tilde{V}_{x_k}(t, \eta)$ of $x_k(t)$ with $g_{\sigma(t)}$, which is (refer to (15))

$$\int_{-\infty}^{\infty} A_k(t + \tau) e^{i2\pi \phi_k(t + \tau)} g_{\sigma(t)}(\tau) e^{-i2\pi \eta \tau} d\tau,$$

can be well-approximated by

$$\int_{-\infty}^{\infty} A_k(t) e^{i2\pi \left(\phi_k(t) + \phi'_k(t) \tau + \frac{1}{2} \phi''_k(t) \tau^2 \right)} g_{\sigma(t)}(\tau) e^{-i2\pi \eta \tau} d\tau, \quad (47)$$

then $\tilde{V}_{x_k}(t, \eta)$ lies within the zone of time-frequency plane:

$$\phi'_k(t) - \alpha \left(\frac{1}{\sigma} + 2\pi |\phi''_k(t)| \sigma \right) \leq \eta \leq \phi'_k(t) + \alpha \left(\frac{1}{\sigma} + 2\pi |\phi''_k(t)| \sigma \right),$$

and hence the well-separable condition for this $x(t)$ is

$$\phi'_{k-1}(t) - \alpha \left(\frac{1}{\sigma} + 2\pi |\phi''_{k-1}(t)| \sigma \right) \leq \phi'_k(t) + \alpha \left(\frac{1}{\sigma} + 2\pi |\phi''_k(t)| \sigma \right), \quad (48)$$

or equivalently

$$a_k(t) \sigma(t)^2 - b_k(t) \sigma(t) + 2\alpha \leq 0, \quad \text{for } k = 2, \dots, K, \quad (49)$$

where

$$a_k(t) = 2\pi \alpha (|\phi''_{k-1}(t)| + |\phi''_k(t)|), \quad b_k(t) = \phi'_k(t) - \phi'_{k-1}(t). \quad (50)$$

If

$$b_k(t)^2 - 8\alpha a_k(t) = (\phi'_k(t) - \phi'_{k-1}(t))^2 - 16\pi \alpha^2 (|\phi''_k(t)| + |\phi''_{k-1}(t)|) \geq 0,$$

then (48) is equivalent to

$$\frac{b_k(t) - \sqrt{b_k(t)^2 - 8\alpha a_k(t)}}{2a_k(t)} \leq \sigma(t) \leq \frac{b_k(t) + \sqrt{b_k(t)^2 - 8\alpha a_k(t)}}{2a_k(t)}, \quad (51)$$

for $k = 2, \dots, K$. Otherwise, if $b_k(t)^2 - 8\alpha a_k(t) < 0$, then there is no suitable solution of the parameter σ for (48) or equivalently (49), which means that components $x_{k-1}(t)$ and $x_k(t)$ of multicomponent signal $x(t)$ cannot be separated in the time-frequency plane. Thus we reach our well-separated condition of STFTs with a time-varying $\sigma = \sigma(t)$.

Theorem 4. Let $x(t) = \sum_{k=1}^K x_k(t)$, where each $x_k(t) = A_k(t)e^{i2\pi\phi_k(t)}$ is a linear chirp signal or its adaptive STFT $\tilde{V}_{x_k}(t, \eta)$ with $g_{\sigma(t)}$ can be well approximated by (47), and $\phi'_{k-1}(t) < \phi'_k(t)$. If for any t with $|\phi''_k(t)| + |\phi''_{k-1}(t)| \neq 0$,

$$4\alpha\sqrt{\pi}\sqrt{|\phi''_k(t)| + |\phi''_{k-1}(t)|} \leq \phi'_k(t) - \phi'_{k-1}(t), \quad k = 2, \dots, K, \text{ and} \quad (52)$$

$$\max_{2 \leq k \leq K} \left\{ \frac{b_k(t) - \sqrt{b_k(t)^2 - 8\alpha a_k(t)}}{2a_k(t)} \right\} \leq \min_{2 \leq k \leq K} \left\{ \frac{b_k(t) + \sqrt{b_k(t)^2 - 8\alpha a_k(t)}}{2a_k(t)} \right\}, \quad (53)$$

then the components of $x(t)$ are well-separable in time-frequency plane in the sense that $\tilde{V}_{x_k}(t, \eta)$, $1 \leq k \leq K$ with $\sigma(t)$ chosen to satisfy (51) lie in non-overlapping regions in the time-frequency plane.

As discussed above, a smaller $\sigma(t)$ gives a sharper synchrosqueezed representation. Thus we should choose $\sigma(t)$ as small as possible. Hence, we propose the linear chirp signal-based choice for σ , denoted by $\sigma_2(t)$, to be

$$\sigma_2(t) = \begin{cases} \max \left\{ \frac{b_k(t) - \sqrt{b_k(t)^2 - 8\alpha a_k(t)}}{2a_k(t)} : 2 \leq k \leq K \right\}, & \text{if } |\phi''_k(t)| + |\phi''_{k-1}(t)| \neq 0, \\ \max \left\{ \frac{2\alpha}{\phi'_k(t) - \phi'_{k-1}(t)} : 2 \leq k \leq K \right\}, & \text{if } \phi''_k(t) = \phi''_{k-1}(t) = 0. \end{cases} \quad (54)$$

where $a_k(t)$ and $b_k(t)$ are defined by (50), and α is defined by (34).

Next we show some experiment results. We consider a two-component LFM signal,

$$y(t) = y_1(t) + y_2(t) = \cos(2\pi(12t + 25t^2)) + \cos(2\pi(34t + 32t^2)), \quad t \in [0, 1], \quad (55)$$

where the number of sampling points is 256, namely the sampling rate is 256Hz. The IFs of $y_1(t)$ and $y_2(t)$ are $\phi'_1(t) = 12 + 50t$ and $\phi'_2(t) = 34 + 64t$, respectively. The top-left figure shows the instantaneous frequencies of $y_1(t)$ and $y_2(t)$. With $\sigma_2(t)$, both the proposed adaptive FSST defined by (21) and 2nd-order adaptive FSST defined by (31) can represent this signal sharply. Here and below, we choose $\lambda = \frac{1}{5}$, and hence α which is defined by (34) and used in (54) is $\alpha \approx 0.2855$. Observe that the 2nd-order adaptive FSST further improves the time-frequency energy concentration of the adaptive FSST. Here we also give the results of conventional FSST defined in [18, 19], and conventional 2nd-order FSST defined in [22]. Observe that the 2nd-order

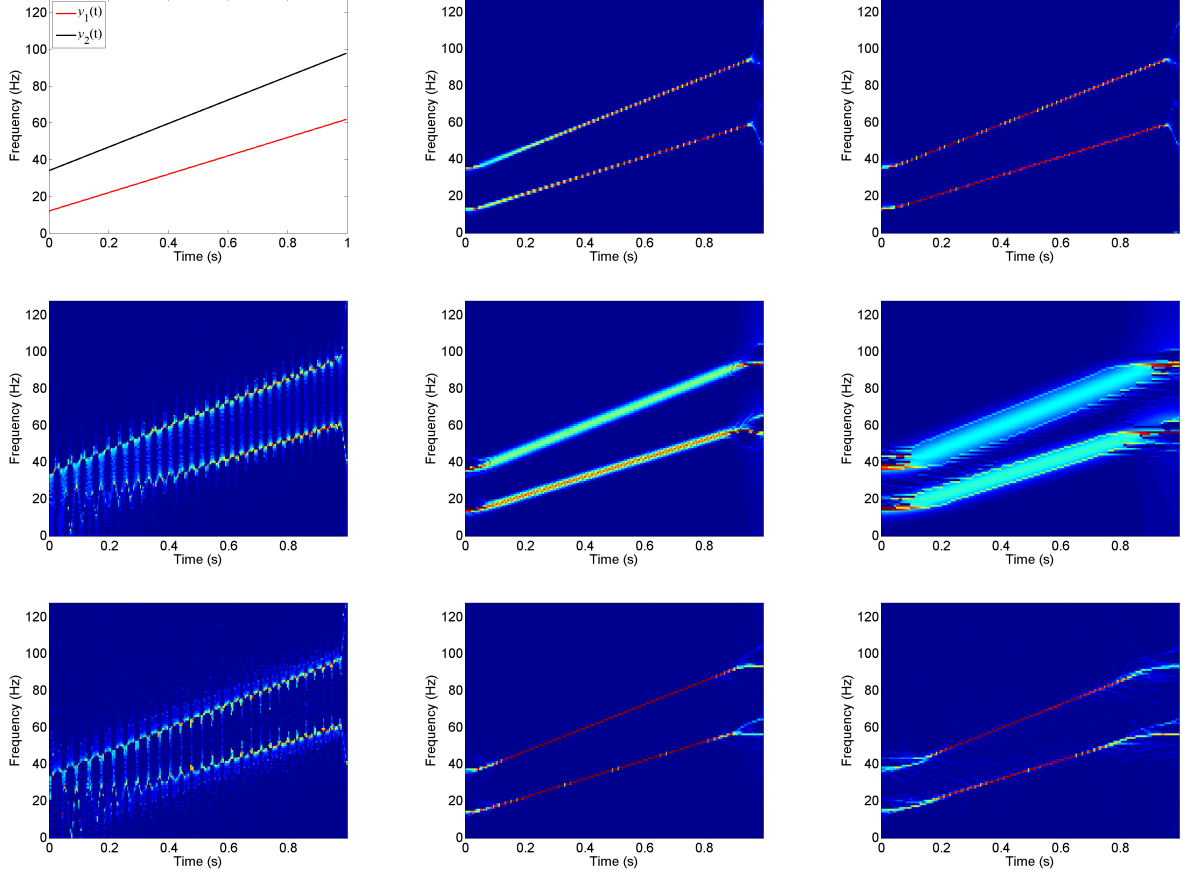


Figure 1: Experiment results on the two-component LFM signal in (55): IFs (Top-left); adaptive FSST with time-varying parameter $\sigma_2(t)$ (Top-middle); 2nd-order adaptive FSST with time-varying parameter $\sigma_2(t)$ (Top-right); conventional FSSTs with $\sigma = 0.01$, $\sigma = 0.05$ and $\sigma = 0.1$ (Middle row, from left to right) and conventional 2nd-order FSSTs with $\sigma = 0.01$, $\sigma = 0.05$ and $\sigma = 0.1$ (Bottom row, from left to right).

FSST is better than the original FSST with the same σ . When $\sigma = 0.01, 0.05$ and 0.1 , the time-frequency representations of conventional 2nd-order FSST are not as sharp or clear as that of the 2nd-order adaptive FSST. Actually, it is hard to find a constant σ to represent non-stationary signals with fast frequency-varying.

6 Selecting the time-varying parameter automatically

Suppose $x(t)$ given by (10) is separable, meaning (52) and (53) hold. If we know $\phi'_k(t)$ and $\phi''_k(t)$, then we can choose a $\sigma(t)$ such as that in (54) to satisfy (51) to define the adaptive STFT and adaptive FSST for sharp representations of $x_k(t)$ in the time-frequency plane and accurate recovery of $x_k(t)$. However in practice, we in general have no prior knowledge of $\phi'_k(t)$ and $\phi''_k(t)$. Hence, we need to have a method which provides suitable $\sigma(t)$. In this paper, we propose an

algorithm for estimation of $\sigma(t)$ which is based on the well-separated condition in (48).

First for temporarily fixed t and σ , denote $V_{x,(t,\sigma)}(\eta) = V_x(t, \eta, \sigma)$, $x(t)$'s STFT with a time-varying parameter defined by (14). We extract the peaks (local maxima) of $|V_{x,(t,\sigma)}(\eta)|$ with certain height. More precisely, assuming $\Gamma_3 > 0$ is a given threshold, we find local maximum points $\eta_1, \eta_2, \dots, \eta_m$ of $|V_{x,(t,\sigma)}(\eta)|$ at which $|V_{x,(t,\sigma)}(\eta)|$ attains local maxima with

$$\frac{|V_{x,(t,\sigma)}(\eta_k)|}{\max |V_{x,(t,\sigma)}(\eta)|} > \Gamma_3, \quad k = 1, \dots, m.$$

Note that m may depend on t and σ . We assume $\eta_1 < \eta_2 < \dots < \eta_m$.

For each local maximum point η_k , we regards η_k is the local maximum of the adaptive STFT $V_{x_k,(t,\sigma)}(\eta)$ of a potential component, denoted by $x_k(t)$ of $x(t)$. To check whether x_k is indeed a component of $x(t)$ or not, we consider the support interval $[l_k, h_k]$ for $V_{x_k,(t,\sigma)}(\eta)$ with $|V_{x_k,(t,\sigma)}(\eta)| > 0$ for $\eta \in [l_k, h_k]$. If there is no overlap among $[l_k, h_k]$, $[l_{k-1}, h_{k-1}]$, $[l_{k+1}, h_{k+1}]$, then we decide that $x_k(t)$ is indeed a component of $x(t)$, where $[l_{k-1}, h_{k-1}]$, $[l_{k+1}, h_{k+1}]$ are the support intervals for x_{k-1} and x_{k+1} defined similarly. With our LMF model, if the estimated IF $\phi'_k(t)$ of $x_k(t)$ is $\hat{c}_k + \hat{r}_k t$, then by (48),

$$h_k = \hat{c}_k + \alpha \left(\frac{1}{\sigma} + 2\pi |\hat{r}_k| \sigma \right), \quad (56)$$

$$l_k = \hat{c}_{k-1} - \alpha \left(\frac{1}{\sigma} + 2\pi |\hat{r}_{k-1}| \sigma \right). \quad (57)$$

Notice that $\hat{c}_k = \eta_k$. Thus we need to estimate the chirp rate \hat{r}_k of $x_k(t)$. To this regard, we extract a small piece of curve in the time-frequency plane passing through (t, η_k) which corresponding to the local ridge on $|V_{x_k,(t,\sigma)}(\eta)|$. More precisely, letting

$$t_{k1} = t - \frac{1}{2} L_{g_\sigma} = t - 2\pi\alpha\sigma, \quad t_{k2} = t + \frac{1}{2} L_{g_\sigma} = t + 2\pi\alpha\sigma,$$

define

$$\hat{d}_k(\tau) = \underset{\eta: \eta \text{ is near } \eta_k}{\operatorname{argmax}} |V_{(\tau,\sigma)}(\eta)|, \quad \tau \in [t_{k1}, t_{k2}].$$

In the above we have used the fact that the duration of $g_\sigma(t)$ is (refer to (34))

$$L_{g_\sigma} = 2\sigma\sqrt{2\ln(1/\epsilon)} = 4\pi\sigma\alpha.$$

Note that $\hat{d}_k(t) = \eta_k$ and (t, η_k) is a point lying on the curve in the time-frequency of (τ, η) given by

$$L = \{(\tau, \hat{d}_k(\tau)) : \tau \in [t_{k1}, t_{k2}]\} = \{(\tau, \eta) : \eta = \hat{d}_k(\tau), \tau \in [t_{k1}, t_{k2}]\}.$$

Most importantly, $\{|V_{x_k,(\tau,\sigma)}(\eta)| : (\tau, \eta) \in L\}$ is the local ridge on $|V_{x_k,(\tau,\sigma)}(\eta)|$ near (t, η_k) , and thus, it is also the local ridge on $|V_x(t, \eta, \sigma)|$. Observe that from STFT of an LFM given by

Proposition 1, the local ridge on $|V_{x_k}(t, \eta, \sigma)|$ occurs when $\phi'_k(t) = c_k + r_k t$. Thus we use the linear function

$$d_k(\tau) = \hat{r}_k(\tau - t) + \hat{c}_k, \tau \in [t_{k1}, t_{k2}]$$

to fit $\hat{d}_k(\tau)$. The obtained \hat{r}_k is the estimated chirp rate r_k of $x_k(t)$. With this \hat{r}_k and $\hat{c}_k = \eta_k$ as given above, we have h_k, l_k given in (56) and (57). Especially when $\hat{r}_k = 0$, recalling the support zone of a sinusoidal signal mode in (35), we have

$$h_k = \hat{c}_k + \frac{\alpha}{\sigma}, l_k = \hat{c}_k - \frac{\alpha}{\sigma}.$$

In this way we obtain the collection of support intervals for $V_x(t, \eta, \sigma)$ for fixed t and σ :

$$\mathbf{s} = \{[l_1, h_1], \dots, [l_m, h_m]\}. \quad (58)$$

If adjacent intervals of \mathbf{s} do not overlap, namely,

$$h_k \leq l_{k+1}, \text{ for all } k = 1, 2, \dots, m-1 \quad (59)$$

holds, then this σ is a right parameter to separate the components and such a σ is a good candidate which we consider to select. Otherwise, if a pair of adjacent intervals of \mathbf{s} overlap, namely, (59) does not hold, then this σ is not the parameter we shall choose and we need to consider a different σ .

In the above description of our idea for the algorithm, we start with a σ and (temporarily fixed) t , then we decide whether this σ is a good candidate to select or not based our proposed criterion: (59) holds or does not. The choice of the initial σ plays a critical role for the success of our algorithm due to the fact that on one hand, as we have mentioned above, in general a smaller σ will result in a sharper representation of SST, and hence, we should find σ as small as possible such that (59) holds; and on the other hand, different σ with which (59) holds may result in different number of intervals m in (58) even for the same time instance t . To keep the number m (the number of components) unchanged when we search for different σ with a fixed t , the initial σ is required to provide a good estimation of the components of a multicomponent signal $x(t)$. To this regard, in this paper we propose to use the Rényi entropy to determine the initial $\sigma(t)$.

The Rényi entropy is a method to evaluate the concentration of a time-frequency representation such as STFT, SST, etc. of a signal of $x(t)$ [41]. Taking STFT $V_x(t, \eta)$ of a signal $x(t)$ as an example, the Rényi entropy with $V_x(t, \eta)$ is

$$E_\zeta(t) = \frac{1}{1-\ell} \log_2 \frac{\int_{t-\zeta}^{t+\zeta} \int_0^\infty |V_x(b, \xi)|^{2\ell} d\xi db}{\left(\int_{t-\zeta}^{t+\zeta} \int_0^\infty |V_x(b, \xi)|^2 d\xi db \right)^\ell}, \quad (60)$$

where ζ and ℓ are positive constants. In this paper we choose $\ell = 2.5$. Note that the smaller the Rényi entropy, the better the time-frequency resolution. So for a fixed time t , we can use (60)

to find a σ (denoted as $\sigma_u(t)$) with the best time-frequency concentration of $V_x(t, \eta, \sigma)$, where $V_x(t, \eta, \sigma)$ is STFT of $x(t)$ defined by (1) with the window function g_σ having a parameter σ . More precisely, replacing $V_x(b, \xi)$ in (60) by $V_x(b, \eta, \sigma)$, we define the Rényi entropy $E_\zeta(t, \sigma)$ of $V_x(t, \eta, \sigma)$, and then, obtain

$$\sigma_u(t) = \underset{\sigma > 0}{\operatorname{argmin}} \{E_\zeta(t, \sigma)\}. \quad (61)$$

We set $\sigma_u(t)$ as the upper bound of $\sigma(t)$ for a fixed t .

With these discussions, we propose an algorithm to estimate $\sigma(t)$ as follows.

Algorithm 1. (Separability parameter estimation) Let $\{\sigma_j, j = 1, 2, \dots, n\}$ be an uniform discretization of σ with $\sigma_1 > \sigma_2 > \dots > \sigma_n > 0$ and sampling step $\Delta\sigma = \sigma_{j-1} - \sigma_j$. The discrete sequence $s(t)$, $t = t_1, t_2, \dots, t_N$ (or $t = 0, 1, \dots, N-1$) is the signal to be analyzed.

Step 1. Let t be one of t_1, t_2, \dots, t_N . Find σ_u in (61) with $\sigma \in \{\sigma_j, j = 1, 2, \dots, n\}$.

Step 2. Let \mathbf{s} be the set of the intervals given by (58) with $\sigma = \sigma_u$. Let $z = \sigma_u$. If (59) holds, then go to Step 3. Otherwise, go to Step 5.

Step 3. Let $\sigma = z - \Delta\sigma$. If the number of intervals m in (58) with this new σ remains unchanged, $\sigma \geq \sigma_n$ and (59) holds, then go to Step 4. Otherwise, go to Step 5.

Step 4. Repeat Step 3 with $z = \sigma$.

Step 5. Let $C(t) = z$, and do Step 1 to Step 4 for different time t of t_1, t_2, \dots, t_N .

Step 6. Smooth $C(t)$ with a low-pass filter $B(t)$:

$$\sigma_{est}(t) = (C * B)(t). \quad (62)$$

We call $\sigma_{est}(t)$ the estimation of the separability time-varying parameter $\sigma_2(t)$ in (54). In Step 6, we use a low-pass filter $B(t)$ to smooth $C(t)$. This is because of the assumption of the continuity condition for $A_k(t)$ and $\phi_k(t)$. With the estimated $\sigma_{est}(t)$, we can define the adaptive STFT, the adaptive FSST and the 2nd-order adaptive FSST with a time-varying parameter $\sigma(t) = \sigma_{est}(t)$.

We use the proposed algorithm to process the two-component linear chirp signal in (55). The different time-varying parameters $\sigma_2(t)$, $\sigma_u(t)$ and $\sigma_{est}(t)$ are shown in the left of Fig.2. Here we let $\sigma \in [0.001, 0.2]$ with $\Delta\sigma = 0.001$, namely $\sigma_1 = 0.2$ in Algorithm 1. We set $\ell = 2.5$, $\zeta = 4$ (sampling points, for discrete signal) and $\Gamma_3 = 0.3$. Note that we set the same values of ℓ , ζ , and Γ_3 for all the following experiments. We use a simple rectangular window $B = \{1/5, 1/5, 1/5, 1/5, 1/5\}$ as the low-pass filter. The estimation $\sigma_{est}(t)$ by Algorithm 1 is very close to $\sigma_2(t)$ except for the start near $t = 0$. So the estimation algorithm is an efficient method to estimate the well-separated time-varying parameter $\sigma_2(t)$. Fig.2 shows the proposed adaptive FSST and 2nd-order adaptive FSST with $\sigma_{est}(t)$.

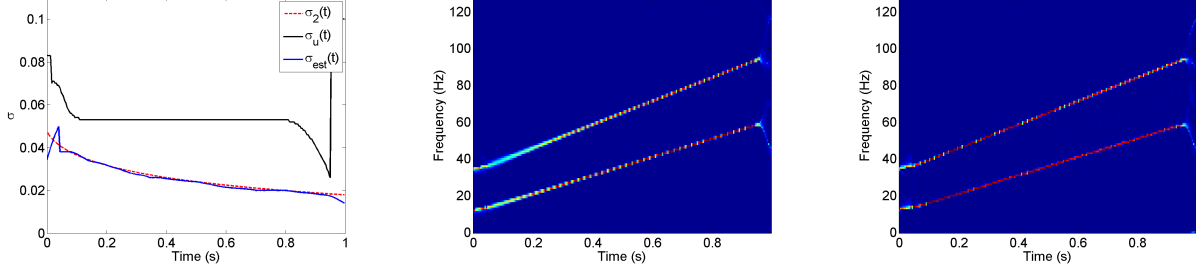


Figure 2: From left to right: Time-varying parameters, adaptive FSST with $\sigma_{est}(t)$, 2nd-order adaptive FSST with $\sigma_{est}(t)$.

7 Experiments and results

In this section, we provide two more numerical examples to further illustrate the effectiveness and robustness of the proposed algorithm.

7.1 Experiments with a three-component synthetic signal

The three-component signal we consider is given by

$$z(t) = z_1(t) + z_2(t) + z_3(t), \quad (63)$$

where

$$\begin{aligned} z_1(t) &= \cos(20\pi(t - 1/3) + 100\pi(t - 1/3)^2), \quad t \in [1/3, 1], \\ z_2(t) &= \cos(74\pi t + 13\cos(4\pi t) + 110\pi t^2), \quad t \in [0, 1], \\ z_3(t) &= \cos(196\pi t + 120\pi t^2), \quad t \in [0, 2/3]. \end{aligned}$$

Note that the durations of the three components in (63) are different. The sampling rate for this experiment is 512Hz. The IFs of the three components are $\phi'_1(t) = 10 + 100(t - 1/3)$, $\phi'_2(t) = 37 - 26\sin(4\pi t) + 110t$ and $\phi'_3(t) = 98 + 120t$, respectively.

The top-left picture of Fig.3 shows the IFs of the three components in $z(t)$. Then we calculate various time-varying parameters as those in Fig.2. The top-right picture of Fig.3 shows the time-varying parameters $\sigma_2(t)$, $\sigma_u(t)$ and $\sigma_{est}(t)$. Again $\sigma_{est}(t)$ is very close to $\sigma_2(t)$. In the bottom row of Fig.3, we show the 2nd-order adaptive FSST with $\sigma_{est}(t)$, and the conventional 2nd-order FSST with a constant $\sigma = 0.05$. Observe that the reassignment result of the conventional 2nd-order FSST does not give sharp representation of the sub-signal with fast varying frequency. Instead, the 2nd-order adaptive FSST not only represents the signal sharply, but also gives better representation for the time-frequency ridges.

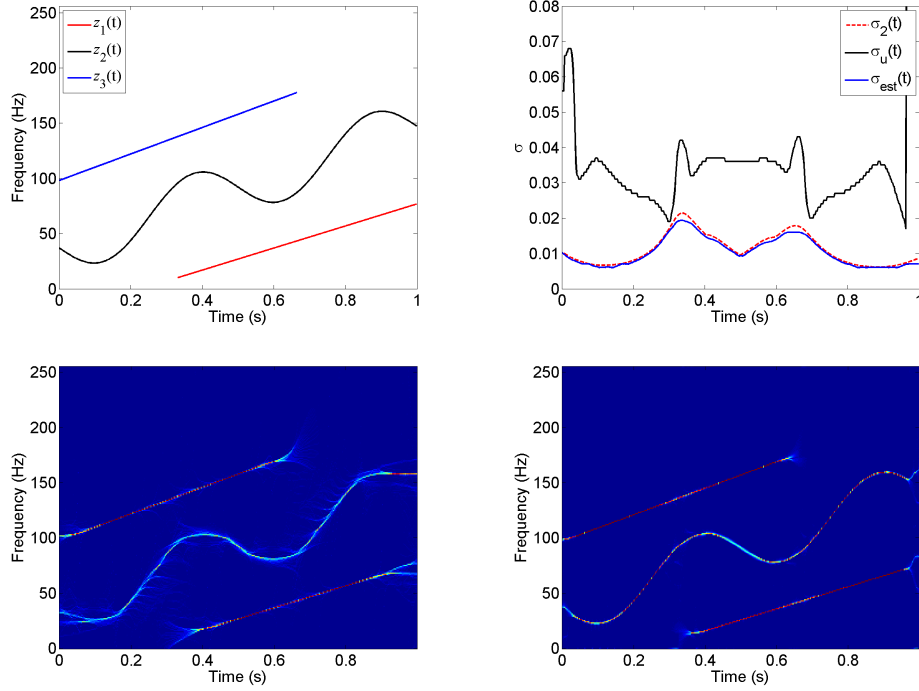


Figure 3: Experiment results on the three-component signal in (63). Top-left: IFs of three components; Top-right: time-varying parameters; Bottom-left: conventional 2nd-order FSST with constant $\sigma = 0.05$; Bottom-right: 2nd-order adaptive FSST with $\sigma_{est}(t)$.

7.2 Application to bat echolocation signal

In order to further verify the reliability of the proposed algorithm, we test our method on a bat echolocation signal emitted by a large brown bat in real world [42]. There are 400 samples with the sampling period 7 microseconds (sampling rate $F_s \approx 142.86$ KHz). From STFT and FSSTs presented in Fig.4, the echolocation signal is a multicomponent signal, which consists of four nonlinear FM components. Recall that compared with other positive constants, $\sigma = 0.05$ works well for $y(t)$ in (55) and $z(t)$ in (63). However, the representations of STFT, conventional SST and 2nd-order SST are very poor if $\sigma = 0.05$. For a given real-world signal, how to select an appropriate constant σ such that the resulting conventional SST or 2nd-order SST has a sharp representation is probably not very simple. Here we choose $\sigma = 8 \times 10^{-5}$, which is close to the mean of $\sigma_{est}(t)$ obtained by Algorithm 1. Fig.4 shows the time-frequency representations of the echolocation signal: STFT, conventional 2nd-order FSST with $\sigma = 8 \times 10^{-5}$ and the 2nd-order adaptive FSST with time-varying parameter $\sigma_{est}(t)$. Unlike the three-component signal in Fig.3, the four components in the bat signal are much well separated. Thus, both the conventional 2nd-order FSST and the 2nd-order adaptive FSST can separate well the components of the signal. In addition, they give sharp representations in the time-frequency plane. Comparing with

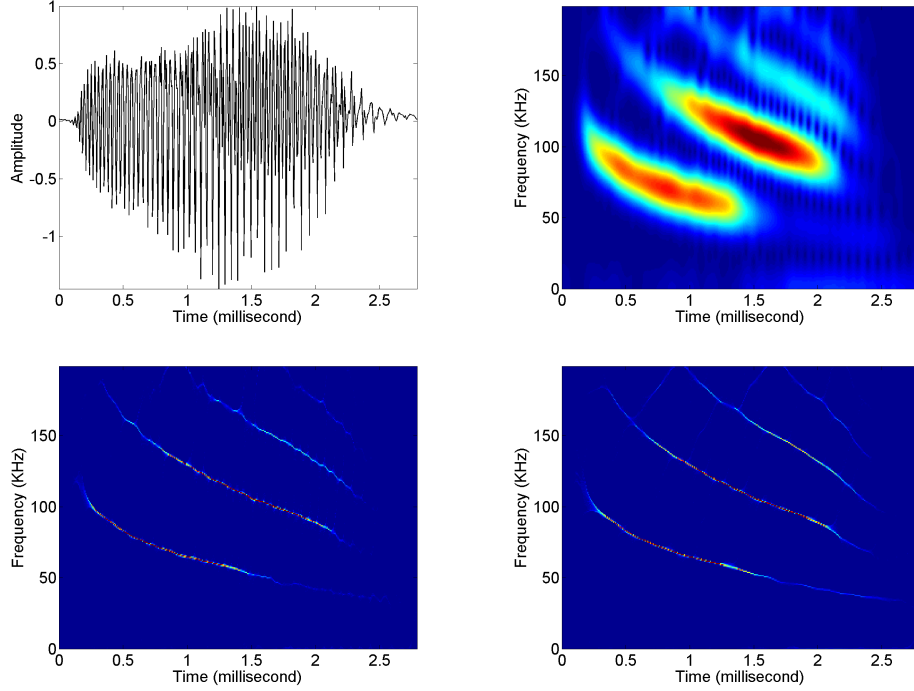


Figure 4: Example of the bat echolocation signal. Top-left: waveform; Top-right: conventional STFT with $\sigma = 8 \times 10^{-5}$; Bottom-left: conventional 2nd-order FSST with $\sigma = 8 \times 10^{-5}$; Bottom-right: 2nd-order adaptive FSST with time-varying parameter $\sigma_{est}(t)$ obtained by our proposed Algorithm 1.

the conventional 2nd-order FSST, the 2nd-order adaptive FSST with $\sigma_{est}(t)$ gives a better representation for the fourth component (the highest frequency component) and the two ends of the signal. Furthermore, $\sigma_{est}(t)$ provides a hint how to select σ for the conventional 2nd-order FSST.

7.3 Signal separation

Final we consider the reconstruction of $z(t)$. Due to the page limitation of the paper, we consider only the three-component signal $z(t)$ in (63) and the 2nd-order FSST. We use (11) and (24) to recover the signal components for conventional 2nd-order FSST and 2nd-order adaptive FSST, respectively. Here we use the maximum values on the FSST plane to search for the IF ridges $\phi'_k(t)$ one by one, see details in [21]. Then integrate around the ridges with $\Gamma = 15$ (discrete value, unitless). In Fig.6 we show the reconstructed components. Essentially there is no error noticeable except for at boundaries of the signals. So our method separates the signals well. We also compare the separation result by our 2nd-order FSST and that by conventional 2nd FSST. Fig.6 provides the differences between the reconstructed components and the original components by these two methods. It is clear our method outperforms the 2nd-order FSST.

We also consider signal separation in noise environment. We add Gaussian noises to the

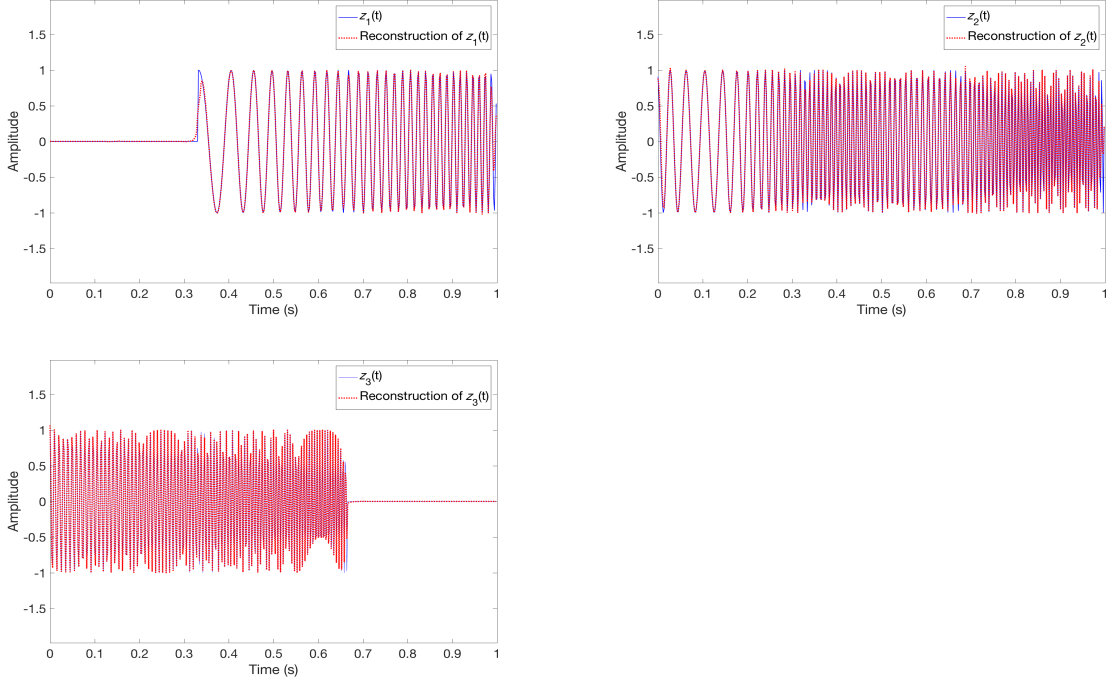


Figure 5: Reconstruction results of the signal in (63). Top-left, top-right and bottom-left: reconstructions of $z_1(t)$, $z_2(t)$ and $z_3(t)$ by 2nd-order adaptive FSST, respectively; Bottom-right: RMSE under different SNRs.

original signal (63) with different signal-to-noise ratios (SNRs). We use the relative “root mean square error” (RMSE) to evaluate the separation performance, which is defined by

$$RMSE = \frac{1}{K} \sum_{k=1}^K \frac{\|z_k - \hat{z}_k\|_2}{\|z_k\|_2}, \quad (64)$$

where \hat{z}_k is the reconstruction result of z_k , K is the number of components. The bottom-right picture of Fig.6 gives the RMSEs of conventional 2nd-order FSST with $\sigma = 0.05$ and 2nd-order adaptive FSST when SNR varies from 10dB to 30dB. Under each SNR, we do Monte-Carlo experiment for 50 runs. Obviously, the reconstruction error of the 2nd-order adaptive FSST is less than that of the conventional 2nd-order FSST.

8 Conclusion

In this paper, we introduce the adaptive STFT with a time-varying parameter and adaptive STFT-based SST (FSST). We also introduce the second order adaptive FSST. We analyze the support zone of STFT for LFM signals, based on which we develop the well-separated condition for multicomponent signals by approximating a multicomponent signal to a mixture of LFM signals

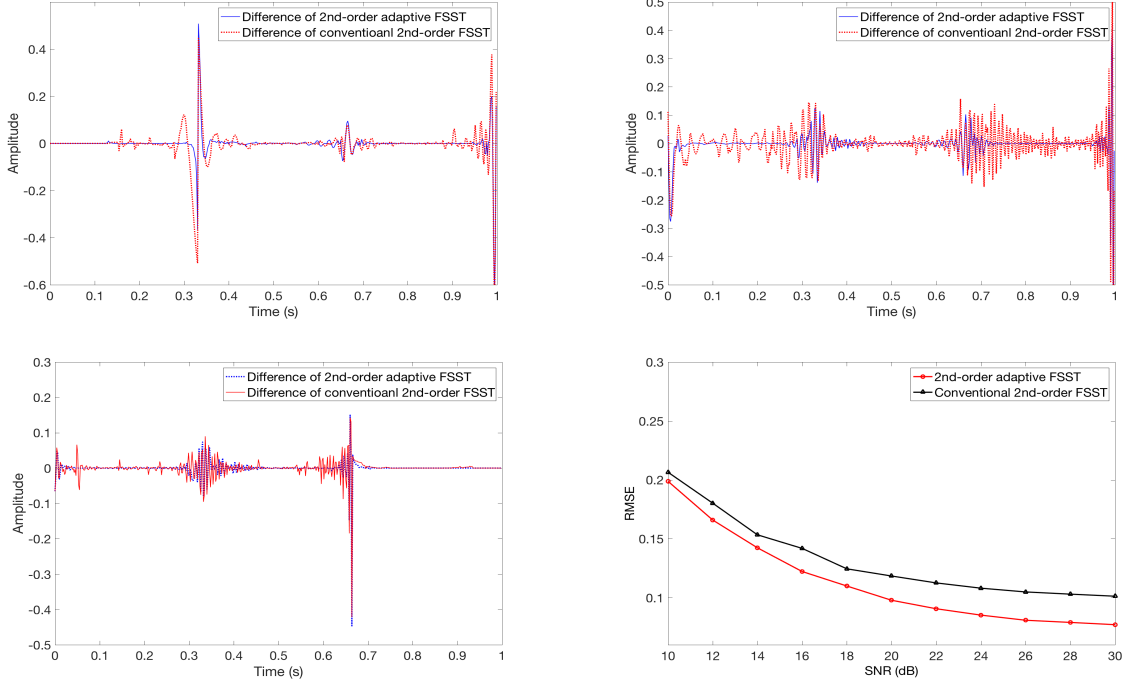


Figure 6: Reconstruction results of the signal in (63). Top-left, top-right and bottom-left: difference of reconstructed $z_j(t)$ with original component $z_j(t)$ by 2nd-order adaptive FSST and conventional 2nd-order FSST, respectively; Bottom-right: RMSE under different SNRs.

during any local time. We propose a method to select the time-varying parameter automatically. The experiments on both synthetic and real data demonstrate that the adaptive FSST is efficient for the instantaneous frequency estimation, sharp representation in the time-frequency and the separation of multicomponent non-stationary signals with fast-varying frequencies. Except for the Gaussian window, further study may focus on other types of time-varying window functions.

Appendix

Proof of Theorem 1. From (3), we have

$$\begin{aligned}
\int_{-\infty}^{\infty} \tilde{V}_x(t, \eta) d\eta &= \int_{-\infty}^{\infty} \int_{-\infty}^{\infty} \hat{x}(\zeta) \hat{g}_{\sigma(t)}(\eta - \zeta) e^{i2\pi t \zeta} d\zeta d\eta \\
&= \int_{-\infty}^{\infty} \hat{x}(\zeta) e^{i2\pi t \zeta} \int_{-\infty}^{\infty} \hat{g}_{\sigma(t)}(\eta - \zeta) d\eta d\zeta \\
&= \int_{-\infty}^{\infty} \hat{x}(\zeta) e^{i2\pi t \zeta} \int_{-\infty}^{\infty} \hat{g}_{\sigma(t)}(\eta) d\eta d\zeta \\
&= \int_{-\infty}^{\infty} \hat{g}_{\sigma(t)}(\eta) e^{i2\pi \cdot 0 \cdot \eta} d\eta \int_{-\infty}^{\infty} \hat{x}(\zeta) e^{i2\pi t \zeta} d\zeta \\
&= g_{\sigma(t)}(0) x(t) = \frac{g(0)}{\sigma(t)} x(t),
\end{aligned}$$

where exchanging the order of $d\eta$ and $d\zeta$ follows from the Fubini's theorem. This shows (16).

To prove (17), note that for real-valued $x(t)$, since $g_{\sigma(t)}(\tau)$ is real-valued, we have

$$\tilde{V}_x(t, -\eta) = \overline{\tilde{V}_x(t, \eta)}.$$

Hence, from (16), we have

$$\begin{aligned}
\frac{g(0)}{\sigma(t)} x(t) &= \int_0^{\infty} \tilde{V}_x(t, \eta) d\eta + \int_{-\infty}^0 \tilde{V}_x(t, \eta) d\eta \\
&= \int_0^{\infty} \tilde{V}_x(t, \eta) d\eta + \int_0^{\infty} \tilde{V}_x(t, -\eta) d\eta \\
&= \int_0^{\infty} \tilde{V}_x(t, \eta) d\eta + \overline{\int_0^{\infty} \tilde{V}_x(t, \eta) d\eta} \\
&= 2\operatorname{Re}\left(\int_0^{\infty} \tilde{V}_x(t, \eta) d\eta\right).
\end{aligned}$$

Thus (17) holds. ■

Proof of Proposition 1. The formula (37) is a special case of (40) with $p = q = 0$. In the following we show (40).

Let $s(t)$ be the linear chirp signal given by (25). Then its STFT with g_σ is

$$\begin{aligned}
V_s(t, \eta) &= \int_{-\infty}^{\infty} s(t + \tau) g_\sigma(\tau) e^{-i2\pi\eta\tau} d\tau \\
&= \int_{-\infty}^{\infty} A e^{p(t+\tau) + \frac{q}{2}(t+\tau)^2 + i2\pi(c(t+\tau) + \frac{1}{2}r(t+\tau)^2)} g_\sigma(\tau) e^{-i2\pi\eta\tau} d\tau \\
&= \frac{A}{\sigma\sqrt{2\pi}} \int_{-\infty}^{\infty} e^{pt + p\tau + \frac{q}{2}t^2 + qt\tau + \frac{q}{2}\tau^2 + i2\pi(ct + c\tau + \frac{r}{2}t^2 + rt\tau + \frac{r}{2}\tau^2)} e^{-\frac{\tau^2}{2\sigma^2}} e^{-i2\pi\eta\tau} d\tau \\
&= \frac{A}{\sigma\sqrt{2\pi}} e^{pt + \frac{q}{2}t^2 + i2\pi(ct + \frac{r}{2}t^2)} \int_{-\infty}^{\infty} e^{-\frac{\tau^2}{2\sigma^2} + \frac{q}{2}\tau^2 + i\pi r\tau^2 + \tau(p + qt + i2\pi(c + rt - \eta))} d\tau \\
&= \frac{A}{\sigma\sqrt{2\pi}} e^{pt + \frac{q}{2}t^2 + i2\pi(ct + \frac{r}{2}t^2)} \frac{\sqrt{\pi}}{\sqrt{\frac{1}{2\sigma^2} - \frac{q}{2} - i\pi r}} e^{\frac{(p + qt + i2\pi(c + rt - \eta))^2}{4(\frac{1}{2\sigma^2} - \frac{q}{2} - i\pi r)}} \\
&= \frac{A}{\sqrt{1 - q\sigma^2 - i2\pi\sigma^2 r}} e^{pt + \frac{q}{2}t^2 + i2\pi(ct + \frac{r}{2}t^2)} e^{-2\pi^2(\eta - c - rt - \frac{p + qt}{i2\pi})^2 \frac{\sigma^2}{1 - q\sigma^2 - i2\pi\sigma^2 r}},
\end{aligned}$$

where in the second last equality, we have applied the following formula (see [1])

$$\int_{-\infty}^{\infty} e^{-(\alpha + i\beta)t^2 + i\omega t} dt = \frac{\sqrt{\pi}}{\sqrt{\alpha + i\beta}} e^{-\frac{\omega^2}{4(\alpha + i\beta)}},$$

for real α and β with $\alpha > 0$. This shows (40) holds. ■

Proof of Theorem 3. For $s = s(t)$ given by (25), from $s'(t) = (p + qt + i2\pi(c + rt))s(t)$ and

$$\tilde{V}_s(t, \eta) = \int_{-\infty}^{\infty} s(t + \tau) \frac{1}{\sigma(t)} g\left(\frac{\tau}{\sigma(t)}\right) e^{-i2\pi\eta\tau} d\tau,$$

we have

$$\begin{aligned}
\frac{\partial}{\partial t} \tilde{V}_s(t, \eta) &= \int_{-\infty}^{\infty} s'(t + \tau) \frac{1}{\sigma(t)} g\left(\frac{\tau}{\sigma(t)}\right) e^{-i2\pi\eta\tau} d\tau + \int_{-\infty}^{\infty} s(t + \tau) \left(-\frac{\sigma'(t)}{\sigma(t)^2}\right) g\left(\frac{\tau}{\sigma(t)}\right) e^{-i2\pi\eta\tau} d\tau \\
&\quad + \int_{-\infty}^{\infty} s(t + \tau) \left(-\frac{\sigma'(t)\tau}{\sigma(t)^3}\right) g'\left(\frac{\tau}{\sigma(t)}\right) e^{-i2\pi\eta\tau} d\tau \\
&= (p + qt + i2\pi(c + rt)) \tilde{V}_s(t, \eta) + (q + i2\pi r) \int_{-\infty}^{\infty} \tau s(t + \tau) \frac{1}{\sigma(t)} g\left(\frac{\tau}{\sigma(t)}\right) e^{-i2\pi\eta\tau} d\tau \\
&\quad - \frac{\sigma'(t)}{\sigma(t)} \tilde{V}_s(t, \eta) - \frac{\sigma'(t)}{\sigma(t)} \tilde{V}_s^{g^2}(t, \eta) \\
&= (p + qt + i2\pi(c + rt) - \frac{\sigma'(t)}{\sigma(t)}) \tilde{V}_s(t, \eta) + (q + i2\pi r) \sigma(t) \tilde{V}_s^{g^1}(t, \eta) - \frac{\sigma'(t)}{\sigma(t)} \tilde{V}_s^{g^2}(t, \eta)
\end{aligned}$$

Thus, if $\tilde{V}_s(t, \eta) \neq 0$, we have

$$\frac{\frac{\partial}{\partial t} \tilde{V}_s(t, \eta)}{\tilde{V}_s(t, \eta)} = p + qt - \frac{\sigma'(t)}{\sigma(t)} + i2\pi(c + rt) + (q + i2\pi r) \sigma(t) \frac{\tilde{V}_s^{g^1}(t, \eta)}{\tilde{V}_s(t, \eta)} - \frac{\sigma'(t)}{\sigma(t)} \frac{\tilde{V}_s^{g^2}(t, \eta)}{\tilde{V}_s(t, \eta)}. \quad (65)$$

Taking partial derivative $\frac{\partial}{\partial \eta}$ to both sides of (65),

$$\frac{\partial}{\partial \eta} \left(\frac{\frac{\partial}{\partial t} \tilde{V}_s(t, \eta)}{\tilde{V}_s(t, \eta)} \right) = (q + i2\pi r) \sigma(t) \frac{\partial}{\partial \eta} \left(\frac{\tilde{V}_s^{g^1}(t, \eta)}{\tilde{V}_s(t, \eta)} \right) - \frac{\sigma'(t)}{\sigma(t)} \frac{\partial}{\partial \eta} \left(\frac{\tilde{V}_s^{g^2}(t, \eta)}{\tilde{V}_s(t, \eta)} \right).$$

Therefore, if in addition, $\frac{\partial}{\partial \eta} \left(\frac{\tilde{V}_s^{g^1}(t, \eta)}{\tilde{V}_s(t, \eta)} \right) \neq 0$, then $(q + i2\pi r) \sigma(t) = P_0(t, \eta)$, where $P_0(t, \eta)$ is defined by (30).

Back to (65), we have

$$\frac{\frac{\partial}{\partial t} \tilde{V}_s(t, \eta)}{\tilde{V}_s(t, \eta)} = p + qt - \frac{\sigma'(t)}{\sigma(t)} + i2\pi(c + rt) + P_0(t, \eta) \frac{\tilde{V}_s^{g^1}(t, \eta)}{\tilde{V}_s(t, \eta)} - \frac{\sigma'(t)}{\sigma(t)} \frac{\tilde{V}_s^{g^2}(t, \eta)}{\tilde{V}_s(t, \eta)}.$$

Hence,

$$\phi'(t) = c + rt = \text{Re} \left\{ \frac{\frac{\partial}{\partial t} \tilde{V}_s(t, \eta)}{i2\pi \tilde{V}_s(t, \eta)} \right\} - \text{Re} \left\{ \frac{\tilde{V}_s^{g^1}(t, \eta)}{i2\pi \tilde{V}_s(t, \eta)} P_0(t, \eta) \right\} + \frac{\sigma'(t)}{\sigma(t)} \text{Re} \left\{ \frac{\tilde{V}_s^{g^2}(t, \eta)}{i2\pi \tilde{V}_s(t, \eta)} \right\}.$$

Thus for an LFM signal $x(t)$ given by (25), at (t, η) where $\frac{\partial}{\partial \eta} \left(\frac{\tilde{V}_x^{g^1}(t, \eta)}{\tilde{V}_x(t, \eta)} \right) \neq 0$ and $\tilde{V}_x(t, \eta) \neq 0$, $\omega_x^{adp, 2nd}(t, \eta)$ defined by (29) is $\phi'(t) = c + rt$, the IF of $x(t)$. This shows Theorem 3. \blacksquare

ACKNOWLEDGMENT: The authors wish to thank Curtis Condon, Ken White, and Al Feng of the Beckman Institute of the University of Illinois for the bat data in Fig.4 and for permission to use it in this paper.

References

- [1] L. Cohen, *Time-frequency Analysis*, Prentice Hall, New Jersey, 1995.
- [2] P. Flandrin, *Time-frequency/Time-scale Analysis*, Wavelet Analysis and Its Applications, vol. 10, Academic Press Inc., San Diego, CA, 1999.
- [3] F. Hlawatsch and G.F. Boudreaux-Bartels, "Linear and quadratic time-frequency signal representations," *IEEE Signal Proc. Magazine*, vol. 9, no. 2, pp. 21–67, 1992.
- [4] S. Mallat, *A Wavelet Tour of Signal Processing*, Academic press, 1999.
- [5] N.E. Huang, Z. Shen, S.R. Long, M.L. Wu, H.H. Shih, Q. Zheng, N.C. Yen, C.C. Tung, and H.H. Liu, "The empirical mode decomposition and Hilbert spectrum for nonlinear and nonstationary time series analysis," *Proc. Roy. Soc. London A*, vol. 454, no. 1971, pp. 903–995, Mar. 1998.

- [6] F. Auger and P. Flandrin, “Improving the readability of time-frequency and time-frequency representations by the reassignment method,” *IEEE Trans. Signal Proc.*, vol. 43, no. 5, pp. 1068–1089, 1995.
- [7] I. Daubechies and S. Maes, “A nonlinear squeezing of the continuous wavelet transform based on auditory nerve models,” in A. Aldroubi, M. Unser Eds. *Wavelets in Medicine and Biology*, CRC Press, 1996, pp. 527–546.
- [8] P. Flandrin, G. Rilling, and P. Goncalves, “Empirical mode decomposition as a filter bank,” *IEEE Signal Proc. Letters*, vol. 11, pp. 112–114, Feb. 2004.
- [9] N.E. Huang and Z. Wu, “A review on Hilbert–Huang transform: Method and its applications to geophysical studies,” *Rev. Geophys.*, vol. 46, no. 2, June 2008.
- [10] G. Rilling and P. Flandrin, “One or two frequencies? The empirical mode decomposition answers,” *IEEE Trans. Signal Proc.*, vol. 56, pp. 85–95, Jan. 2008.
- [11] Z. Wu and N.E. Huang, “Ensemble empirical mode decomposition: A noise-assisted data analysis method,” *Adv. Adapt. Data Anal.*, vol. 1, no. 1, pp. 1–41, Jan. 2009.
- [12] L. Li and H. Ji, “Signal feature extraction based on improved EMD method,” *Measurement*, vol. 42, pp. 796–803, June 2009.
- [13] L.Lin, Y. Wang, and H.M. Zhou, “Iterative filtering as an alternative algorithm for empirical mode decomposition,” *Adv. Adapt. Data Anal.*, vol. 1, no. 4, pp. 543–560, Oct. 2009.
- [14] T. Oberlin, S. Meignen, and V. Perrier, “An alternative formulation for the empirical mode decomposition,” *IEEE Trans. Signal Proc.*, vol. 60, no. 5, pp. 2236–2246, May 2012.
- [15] K. Dragomiretskiy and D. Zosso, “Variational mode decomposition,” *IEEE Trans. Signal Proc.*, vol. 62, no. 3, pp. 531–544, Feb. 2014.
- [16] A. Cicone, J.F. Liu, and H.M. Zhou, “Adaptive local iterative filtering for signal decomposition and instantaneous frequency analysis,” *Appl. Comput. Harmon. Anal.*, vol. 41, no. 2, pp. 384–411, Sep. 2016.
- [17] I. Daubechies, J. Lu, and H.-T. Wu, “Synchrosqueezed wavelet transforms: An empirical mode decomposition-like tool,” *Appl. Comput. Harmon. Anal.*, vol. 30, no. 2, pp. 243–261, Mar. 2011.
- [18] G. Thakur and H.-T. Wu, “Synchrosqueezing based recovery of instantaneous frequency from nonuniform samples,” *SIAM J. Math. Anal.*, vol. 43, no. 5, pp. 2078–2095, 2011.

- [19] T. Oberlin, S. Meignen, and V. Perrier, “The Fourier-based synchrosqueezing transform,” in *Proc. 39th Int. Conf. Acoust., Speech, Signal Proc. (ICASSP)*, 2014, pp. 315–319.
- [20] D. Iatsenko, P.-V. E. McClintock, and A. Stefanovska, “Linear and synchrosqueezed time-frequency representations revisited: Overview, standards of use, resolution, reconstruction, concentration, and algorithms,” *Digital Signal Proc.*, vol. 42, pp. 1–26, July 2015.
- [21] S. Meignen, D.-H. Pham, and S. McLaughlin, “On demodulation, ridge detection and synchrosqueezing for multicomponent signals,” *IEEE Trans. Signal Proc.*, vol. 65, no. 8, pp. 2093–2103, Apr. 2017.
- [22] T. Oberlin, S. Meignen, and V. Perrier, “Second-order synchrosqueezing transform or invertible reassignment? Towards ideal time-frequency representations,” *IEEE Trans. Signal Proc.*, vol. 63, no. 5, pp. 1335–1344, Mar. 2015.
- [23] T. Oberlin and S. Meignen, “The 2nd-order wavelet synchrosqueezing transform,” in *2017 IEEE International Conference on Acoustics, Speech and Signal Processing (ICASSP)*, March 2017, New Orleans, LA, USA.
- [24] R. Behera, S. Meignen, and T. Oberlin, “Theoretical analysis of the 2nd-order synchrosqueezing transform,” *Appl. Comput. Harmon. Anal.*, vol. 45, no. 2, pp. 379–404, Sep. 2018.
- [25] D.-H. Pham and S. Meignen, “High-order synchrosqueezing transform for multicomponent signals analysis - With an application to gravitational-wave signal,” *IEEE Trans. Signal Proc.*, vol. 65, no. 12, pp. 3168–3178, June 2017.
- [26] C. Li and M. Liang, “A generalized synchrosqueezing transform for enhancing signal time-frequency representation,” *Signal Proc.*, vol. 92, no. 9, pp. 2264–2274, 2012.
- [27] C.K. Chui and M.D. van der Walt, “Signal analysis via instantaneous frequency estimation of signal components,” *Int’l J. Geomath.*, vol. 6, no. 1, pp. 1–42, Apr. 2015.
- [28] H.Z. Yang, “Synchrosqueezed wave packet transforms and diffeomorphism based spectral analysis for 1D general mode decompositions,” *Appl. Comput. Harmon. Anal.*, vol. 39, no. 1, pp. 33–66, 2015.
- [29] C.K. Chui, Y.-T. Lin, and H.-T. Wu, “Real-time dynamics acquisition from irregular samples - with application to anesthesia evaluation,” *Anal. Appl.*, vol. 14, no. 4, pp. 537–590, July 2016.

- [30] I. Daubechies, Y. Wang, and H.-T. Wu, “ConceFT: Concentration of frequency and time via a multitapered synchrosqueezed transform,” *Phil. Trans. Royal Soc. A*, vol. 374, no. 2065, Apr. 2016.
- [31] S. Wang, X. Chen, G. Cai, B. Chen, X. Li, and Z. He, “Matching demodulation transform and synchrosqueezing in time-frequency analysis,” *IEEE Trans. Signal Proc.*, vol. 62, no. 1, pp. 69–84, Jan. 2014.
- [32] Q.T. Jiang and B.W. Suter, “Instantaneous frequency estimation based on synchrosqueezing wavelet transform,” *Signal Proc.*, vol. 138, no. pp.167–181, 2017.
- [33] C.K. Chui and H.N. Mhaskar, “Signal decomposition and analysis via extraction of frequencies,” *Appl. Comput. Harmon. Anal.*, vol. 40, no. 1, pp. 97–136, 2016.
- [34] L. Li, H. Cai, Q. Jiang, and H. Ji, “An empirical signal separation algorithm for multi-component signals based on linear time-frequency analysis,” preprint, 2017. Available at <http://www.math.umsl.edu/~jiang>
- [35] D.L. Jones and R.G. Baraniuk, “A simple scheme for adapting time-frequency representations,” *IEEE Trans. Signal Proc.*, vol. 42, no. 12, pp. 3530–3535, Dec. 1994.
- [36] N. Czerwinski and D.L. Jones, “Adaptive short-time Fourier analysis,” *IEEE Signal Proc. Letters*, vol. 4, no. 2, pp. 42–45, Feb. 1997.
- [37] V. Katkovnik and L. Stanković, “Instantaneous frequency estimation using the Wigner distribution with varying and data-driven window length,” *IEEE Trans. Signal Proc.*, vol. 46, no. 9, pp. 2315–2325, Sep. 1998.
- [38] J.G. Zhong and Y. Huang, “Time-frequency representation based on an adaptive short-time Fourier transform,” *IEEE Trans. Signal Proc.*, vol. 58, no. 10, pp. 5118–5128, Oct. 2010.
- [39] Y.-L. Sheu, L.-Y. Hsu, P.-T. Chou, and H.-T. Wu, “Entropy-based time-varying window width selection for nonlinear-type time-frequency analysis,” *Int’l J. Data Sci. Anal.*, vol. 3, pp. 231–245, 2017.
- [40] A. Berrian and N. Saito, “Adaptive synchrosqueezing based on a quilted short-time Fourier transform,” arXiv:1707.03138v5, Sep. 2017.
- [41] L. Stankovic, “A measure of some time-frequency distributions concentration,” *Signal Proc.*, vol. 81, no. 3, pp. 621–631, 2001.
- [42] <http://dsp.rice.edu/software/bat-echolocation-chirp>.